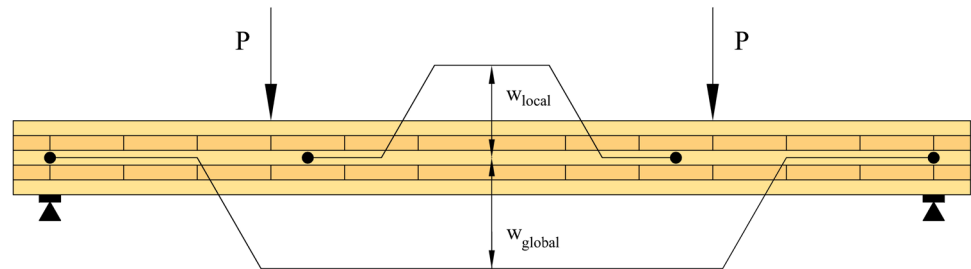




LUND
UNIVERSITY



EVALUATION OF A TESTING METHOD FOR SHEAR STIFFNESS PROPERTIES FOR CROSS LAMINATED TIMBER

CALLE LIND

Structural
Mechanics

Master's Dissertation

DEPARTMENT OF CONSTRUCTION SCIENCES
DIVISION OF STRUCTURAL MECHANICS

ISRN LUTVDG/TVSM--22/5259--SE (1-65) | ISSN 0281-6679

MASTER'S DISSERTATION

EVALUATION OF A TESTING METHOD FOR SHEAR STIFFNESS PROPERTIES FOR CROSS LAMINATED TIMBER

CALLE LIND

Supervisors: Dr **HENRIK DANIELSSON**, Division of Structural Mechanics, LTH,
ANDREAS GUSTAFSSON, Lic Eng, WSP Sverige AB and **DANIEL ANDERSON**, MSc, Södra.

Examiner: Professor **ERIK SERRANO**, Division of Structural Mechanics, LTH.

Copyright © 2022 Division of Structural Mechanics,
Faculty of Engineering LTH, Lund University, Sweden.

Printed by V-husets tryckeri LTH, Lund, Sweden, June 2022 *(Pl)*.

For information, address:

Division of Structural Mechanics,
Faculty of Engineering LTH, Lund University, Box 118, SE-221 00 Lund, Sweden.

Homepage: www.byggmek.lth.se

Abstract

Cross laminated timber (CLT) is an engineered wood product that was first developed in the 1990s. Since then it has grown in popularity thanks to its many advantages such as: low environment impact, high degree of prefabrication and low weight. As the material is relatively new the standardization process is still in the early stages. The purpose of this thesis is to evaluate a testing method which is suggested to be part of the standardization of CLT.

The testing method, which is described in the European standard EN 16351, is a four-point bending test with the purpose to determine, among other properties, the rolling shear modulus of the transverse layers in CLT. The test is performed by measuring the so called local- and global deflections. The local deflection is measured between the two loads and is assumed to depend only on bending and is used to estimate the bending stiffness of the beam. The global deflection is measured for the entire span and is therefore dependent on both bending and shear. The global deflection is used to estimate the so called apparent bending stiffness.

By determining the local- and apparent bending stiffness the shear stiffness of the entire cross section can be determined. When the shear stiffness of the entire cross section is determined the shear modulus for the transverse layers (rolling shear modulus) can be determined by applying Timoshenko beam theory and subtracting the contribution of the shear modulus of the longitudinal layers.

For this project no laboratory testing was performed, the testing method was instead evaluated with Finite Element-models (FE-models). When analysing with FE-models the rolling shear modulus is known beforehand since it is used as an input parameter to the models. The accuracy of the test method was evaluated by comparing the calculated rolling shear modulus to the input rolling shear modulus. An accurate result should result in the output and input being equal.

The results indicated that the method used to determine the rolling shear modulus is largely influenced by assumptions made according to Timoshenko beam theory. One of these assumptions include the shear correction factor, which is used to correct a theoretical assumption that results in an overestimated shear stiffness. The shear correction factor according to beam theory results in inaccurate results, but the factor can be altered to correlate better with the expected rolling shear modulus. One of the problems with such a procedure is that the rolling shear modulus must be known beforehand to do an accurate alteration. Other deviations between beam theory and the FE-models affecting the results include: boundary conditions and shear strain distributions.

Keywords : CLT, cross laminated timber, EN 16351, four-point bending, rolling shear modulus, FE-modelling

Acknowledgements

First of all I would like to express my gratitude to my supervisor Henrik Danielsson for his support and guidance throughout this project. Our meetings and discussions have been really interesting and essential for the proceedings of the project.

I would also like to thank my supervisor from WSP, Andreas Gustafsson, my examiner Erik Serrano and Daniel Anderson from Södra. Your commitment and interest of this project have been encouraging and helped me forward.

Many thanks to my classmates for their great friendship throughout my five years at LTH. A special thanks to my opponent Erik Lundin, both for being a good friend and for your input to my work. Writing our dissertations together at WSP has been a fun and inspiring period of time.

Lastly I would like to thank my family and my girlfriend Lovisa for always being there for me and for your support throughout my entire education.

30th May, 2022

Lund, Sweden

A handwritten signature in cursive script, reading "Calle L.", positioned above a horizontal line.

Calle Lind

Notations and Symbols

Latin letters

L	Longitudinal direction.
R	Radial direction.
T	Tangential direction.
x	Global x -direction of the CLT-beam.
y	Global y -direction of the CLT-beam.
z	Global z -direction of the CLT-beam.
E	Young's modulus (modulus of elasticity).
G	Shear modulus.
E_L	Young's modulus parallel to grain.
E_R	Young's modulus perpendicular to grain in R -direction.
E_T	Young's modulus perpendicular to grain in T -direction.
G_{LR}	Shear modulus parallel to grain (LR -plane).
G_{LT}	Shear modulus parallel to grain (LT -plane).
G_{RT}	Rolling shear modulus.
I_{net}	Net moment of inertia.
I_{ef}	Effective moment of inertia.
D_{GA}	Cross section shear stiffness.
V	Shear force.
M	Moment.
P	Load.
L	Span length.
w	Deformation (vertical deflection).
$W_{x,net}$	Net moment of resistance.
$S_{x,v}$	Net static moment for longitudinal layers.
$S_{x,Rv}$	Net static moment for transverse layers.
w_l	Local deflection.
w_g	Global deflection.
$(EI)_{local,net}$	Local bending stiffness determined by measured deflections.
$(EI)_{app,net}$	Apparent bending stiffness determined by measured deflections.
\mathbf{K}	Stiffness matrix.
\mathbf{f}	Force vector.
\mathbf{a}	Result vector.
\mathbf{K}^e	Element stiffness matrix.
\mathbf{f}^e	Element force vector.

Greek letters

ν	Poisson's ratio.
γ_i	Gamma-factor.
κ	Shear correction factor.
θ	Rotation.
γ	Shear strain.
σ	Stress vector.
ε	Strain vector.
C	Compliance matrix.
D	Constitutive matrix.
$\sigma_{m,x}$	Normal stress in x -direction.
$\tau_{v,xz}$	Longitudinal shear stress.
$\tau_{Rv,xz}$	Rolling shear stress.

Contents

Abstract	I
Acknowledgements	III
Notations and Symbols	V
Table of Contents	VIII
1 Introduction	1
1.1 Context	1
1.2 Aim and objective	2
1.3 Method	2
2 Background	3
2.1 Wood as a structural material	3
2.1.1 Wood species	4
2.1.2 Strength and stiffness properties of wood	5
2.1.3 Shear stiffness properties	8
2.2 Cross Laminated Timber	9
2.3 Beam theory	10
2.3.1 Bernoulli Euler beam theory and Gamma-method	11
2.3.2 Timoshenko theory	13
2.4 Testing method	14
2.4.1 Evaluation of test results	18
2.5 Finite element method	21
3 Method	23
3.1 Deformation calculations	23
3.1.1 Calfem	23
3.2 Finite element modelling	26
3.2.1 2D-model	27
3.2.2 Convergence study	29
3.3 Evaluation of FE-models	31
3.3.1 Parametric study	32
4 Results	39
4.1 Evaluation of test	40
4.1.1 Homogeneous beams	40
4.1.2 CLT-beams	46

5 Discussion and Conclusions	53
5.1 Concluding remarks	53
5.2 Further analysis	56
Bibliography	57

1 Introduction

1.1 Context

Cross Laminated Timber (CLT) (see Figure 1.1) is a relatively new engineered wood product, that was first developed in Central Europe and was introduced to Sweden in the late 1990s. Since then, the product has become more and more popular thanks to its many advantages [1]. CLT offers high strength and high stiffness in comparison to its low weight and allows for a high degree of prefabrication which gives a shorter erection phase. Another general advantage that is often highlighted is the low environmental impact compared to other materials such as concrete and steel.

Despite the increasing popularity and the many advantages of CLT the product is still in the early stages of standardization when it comes to determining the mechanical properties. The standardization of CLT started in Europe in 2008 and the first European standard for CLT, EN 16351 was released in 2014 [2]. The standard is however not yet accepted as basis for CE-marking, which is a European product certification that is needed for some products (including CLT) to be sold in the European Union [3].

The current European assessment document (EAD) [4] for solid wood elements was released in 2015. In the EAD, several methods are described for assessing performance of CLT in relation to the characteristics of the product. The method described for bending properties is a four-point bending test of a plate. One assumption made for the test is to set the shear modulus of the transverse planes to 50 MPa [4]. This shear modulus is called rolling shear and is typically many times lower than the longitudinal shear modulus. The rolling shear modulus, like many other material properties, display uncertainties when being measured. Inaccurate assumptions of the rolling shear stiffness could in turn lead to inaccurate testing results and performance.

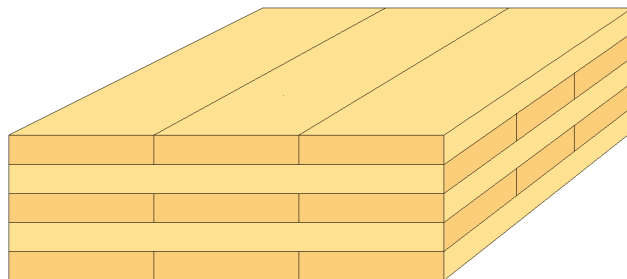


Figure 1.1: Sketch of a five layered CLT element.

The fact that the standardization of CLT is in the early stages, means many new standards and testing methods are still under evaluation, including the four-point bending test regarding rolling shear strength and stiffness referred to in the current EAD [4] and further described in EN 16351 Annex C [5].

1.2 Aim and objective

The aim of this work is to perform a thorough evaluation of one of the testing methods for shear strength and stiffness in EN 16351 – The four-point bending set up. The evaluation will be made to investigate if this testing method is suitable for determining the shear properties, especially the rolling shear modulus. The evaluation also includes investigations of how different parameters affect the shear stiffness, in particular rolling shear, and which parameters that affect the results the most. The parameters of main interest are the input variables of the equations used to evaluate the testing method described in EN 16351 Annex C [5]. Further investigated parameters include

- The effect of the ratio between the thickness and the width of the lamellas.
- The effect of using wood species with different properties.
- The effect of the annual growth ring pattern.

1.3 Method

The first part of the project consisted of a literature study. The study was performed to gather information on the topic and to understand what is known of it today. The information includes; mechanical stiffness and strength properties of different softwood and hardwood species, the effect of rolling shear and technical documents from testing according to EN 16351.

Calculations were performed according to beam theory and using 2D FE-models. Calculations regarding shear force capacity with respect to rolling shear stress (in the transverse layers) for a CLT element in four point bending was performed according to Bernoulli-Euler and Timoshenko theory. A model of the test set-up for shear strength and stiffness according to EN 16351 was made with the FE-software Abaqus, to be compared to the calculations using beam theory. The four-point bending test was not tested with a physical CLT element in the laboratory. The evaluation was instead based on the calculations and the FE-models.

The model in Abaqus was also made to perform a parameter study of the CLT specimen in the four-point bending test. A Python script was used to generate CLT models where parameters such as lamella ratios, wood properties etc could easily be changed (Python is the programming language that Abaqus is based on).

2 Background

2.1 Wood as a structural material

Softwood, which is the most common timber material used in construction, is mainly built up by tube-shaped cells called *tracheids*. These cells build up the tissue of the wood called fibre or grain. The tracheids have a function to distribute water for a living tree, the cells are therefore oriented in the longitudinal direction of the tree i.e. from the root to the treetop [6].

The need for water and nutrition varies throughout the year. The growing process of the tree takes place during the spring and the need for water and nutrition is therefore high. To cope with this the tube-shaped cells that are formed during the spring have thin cell walls that give the cell a larger tube diameter which allows for higher water transportation. The cells that are formed during this time constitute the so called earlywood [6].

When the growing process is finished, the need for water and nutrition transportation decreases. The cells that are formed during the summer and fall are instead optimized to withstand harsh weather in form of strong winds and snow loads. These cells constitute the so called latewood and have thicker cell walls and smaller cell cavities. The two different cell types that are formed during a year make a structural pattern of earlywood and latewood called annual growth rings (see Figure 2.1).

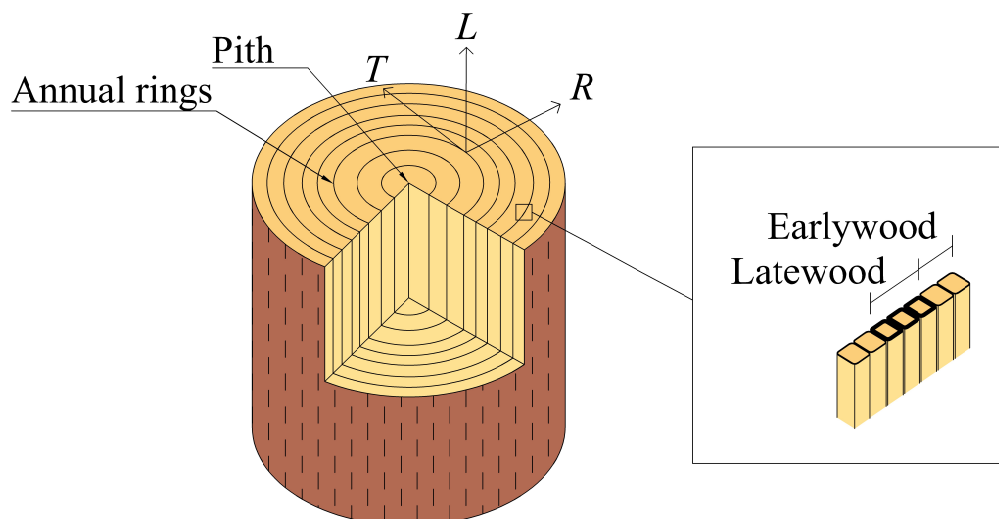


Figure 2.1: Cross section of a log showing earlywood- and latewood cells and how they build up the annual rings. The three main axes are also shown.

Since latewood cells have thicker cell walls and therefore higher strength compared to earlywood cells the proportion between the two is of large influence for the mechanical properties of wood [6]. This is further discussed in Section 2.1.3.

Hardwood (see Section 2.1.1) has a more complicated cell structure compared to softwood [6]. While softwood is mainly built up by tracheids, hardwood consist of a more complex set of cells. The four main cells types are *fibers*, *vessels*, *tracheids* and *parenchyma* cells [7]. All cells serve different purposes, but the fiber cells are of greatest interest from a mechanical perspective since they contribute most to the mechanical stiffness and strength of the material. The function of the vessel cells is to transport water. The vessels can be seen as pores under a microscope [7]. The material around the pores makes up a more dense material compared to softwood where the water transportation is carried out by the tracheids, which do not have any pores.

Hardwood species often have higher mass density compared to softwood species and generally have better fire resistance compared to softwood species. The usage of hardwood for structural timber is however not as common as softwood. Reasons for this include hardwood being more expensive and sometimes more difficult to work with. Other reasons are discussed in Section 2.1.1. Hardwood is more commonly seen in high-quality furniture and flooring. Typical hardwood species are oak, birch and beech.

2.1.1 Wood species

The most common wood species in Sweden are Norway spruce and Scots pine, with 39.7 % and 39.3 % of the total growing stock respectively [8]. These are specified as softwood species and are also the most common species used in engineered wood products [1]. The most common hardwood species in Sweden is Birch, which accounts for 12.9 % of the total growing stock [8].

Softwood comes from coniferous trees and are green all year around, while hardwood is from broad-leaved trees and usually lose their leaves during the winter months. To reach a suitable size for timber production, softwood species typically take around 20-30 years of growth. Compared to some hardwood species, which take over 100 years to reach a suitable size, softwood species generally grow significantly faster [9]. The growth rate however varies between species.

The fact that softwood species in general are more common and often grow faster compared to hardwood species are two reasons why they are more commonly used as a building material. Another reason is the development of the paper industry in the beginning of the 19th century. Softwood species were seen to have a better morphology for making paper and where therefore cultivated to a larger extent compared to hardwood species. Since the paper- and timber industry are connected to each other this came to influence which species that were used for structural timber then and still is today [7]. Hardwood have properties that might be more favourable in a load bearing structure, e.g. higher density and usually higher rolling shear strength [9].

Norway spruce is the most important wood species in Europe when it comes to use for

load-bearing timber structures today. But to only cultivate one species is not good for biodiversity. This has become an increasing issue due to climate change and pressure is being put on the industry to use a variety of softwood and hardwood. Hardwood therefore has a high potential to be used more for structural timber in the future [10].

2.1.2 Strength and stiffness properties of wood

The mechanical properties of wood are determined by the cell structure described in Section 2.1. The tube-shaped cells have a higher strength in compression and tension parallel to grain than perpendicular to grain. Wood thus has different properties depending on which direction it is being loaded [6]. For wood there are three main axes described as (see Figure 2.1)

- L = The longitudinal axis which is parallel to the grain.
- T = The tangential axis which is tangential to the annual rings.
- R = The radial axis which is radial to the annual rings.

Each of the three main axes has different properties when being subjected to loads. This is the definition of an orthotropic material. To describe the linear relation between the stress and strain in local coordinates for an orthotropic material, the following relations can be used

$$\boldsymbol{\sigma} = \mathbf{D}\boldsymbol{\varepsilon} \quad (2.1)$$

$$\boldsymbol{\varepsilon} = \mathbf{D}^{-1}\boldsymbol{\sigma} = \mathbf{C}\boldsymbol{\sigma} \quad (2.2)$$

where $\boldsymbol{\sigma}$ is the stress vector and $\boldsymbol{\varepsilon}$ is the strain vector given by

$$\boldsymbol{\sigma} = [\sigma_{LL} \quad \sigma_{RR} \quad \sigma_{TT} \quad \tau_{LR} \quad \tau_{LT} \quad \tau_{RT}]^T \quad (2.3)$$

$$\boldsymbol{\varepsilon} = [\varepsilon_{LL} \quad \varepsilon_{RR} \quad \varepsilon_{TT} \quad \gamma_{LR} \quad \gamma_{LT} \quad \gamma_{RT}]^T \quad (2.4)$$

and where $\mathbf{C} = \mathbf{D}^{-1}$ is the compliance matrix and given by

$$\mathbf{C} = \begin{bmatrix} \frac{1}{E_L} & -\frac{\nu_{RL}}{E_R} & -\frac{\nu_{TL}}{E_T} & 0 & 0 & 0 \\ -\frac{\nu_{LR}}{E_L} & \frac{1}{E_R} & -\frac{\nu_{TR}}{E_T} & 0 & 0 & 0 \\ -\frac{\nu_{LT}}{E_L} & -\frac{\nu_{RT}}{E_R} & -\frac{1}{E_T} & 0 & 0 & 0 \\ 0 & 0 & 0 & \frac{1}{G_{LR}} & 0 & 0 \\ 0 & 0 & 0 & 0 & \frac{1}{G_{LT}} & 0 \\ 0 & 0 & 0 & 0 & 0 & \frac{1}{G_{RT}} \end{bmatrix} \quad (2.5)$$

To describe wood in the elastic range, twelve constants are necessary. These twelve constants are implemented in the compliance matrix \mathbf{C} , and are the modulus of elasticity in each main direction, E_L , E_R , E_T , the shear modulus in each plane of the main directions, G_{LR} , G_{LT} , G_{RT} , and six Poisson's ratios, ν_{LR} , ν_{LT} , ν_{RT} , ν_{RL} , ν_{TL} , and ν_{TR} [6]. For linear elasticity, the Poisson's ratios are assumed to be pair-wise equal according to [6]

$$\frac{\nu_{LR}}{E_L} = \frac{\nu_{RL}}{E_R}, \quad \frac{\nu_{LT}}{E_L} = \frac{\nu_{TL}}{E_T}, \quad \frac{\nu_{RT}}{E_R} = \frac{\nu_{TR}}{E_T} \quad (2.6)$$

This reduces the number of constants to nine and also results in symmetrical \mathbf{C} and \mathbf{D} matrices. For the two-dimensional case, the stresses or strains in the out-of-plane direction are negligible small. The conditions of *plane stress* or *plane strain* can therefore be applied, meaning, either in-plane stresses or in-plane strains exist. The stress and strain relation in local coordinates for plane stress reduces to

$$\boldsymbol{\sigma} = \mathbf{D}\boldsymbol{\varepsilon} \quad (2.7)$$

$$\boldsymbol{\varepsilon} = \mathbf{D}^{-1}\boldsymbol{\sigma} = \mathbf{C}\boldsymbol{\sigma} \quad (2.8)$$

$$\boldsymbol{\sigma} = [\sigma_{ii} \quad \sigma_{jj} \quad \tau_{ij}]^T \quad (2.9)$$

$$\boldsymbol{\varepsilon} = [\varepsilon_{ii} \quad \varepsilon_{jj} \quad \gamma_{ij}]^T \quad (2.10)$$

$$\mathbf{C} = \begin{bmatrix} \frac{1}{E_i} & -\frac{\nu_{ji}}{E_j} & 0 \\ -\frac{\nu_{ij}}{E_i} & \frac{1}{E_j} & 0 \\ 0 & 0 & \frac{1}{G_{ij}} \end{bmatrix} \quad (2.11)$$

The indices i and j denote the local ij -coordinate system (e.g. of the lamellas that make up a CLT-beam).

The strength and stiffness properties differ from wood species to wood species. The wood species of interest in this thesis are Norway spruce, birch and beech. Birch and beech are both hardwood species and not as common in timber products. Scots pine, which is also common in timber products, is not evaluated due to its properties being similar to those of Norway spruce. The nine property constants for the different wood species are described in Table 2.1, data that was not found is marked as $-$. The parameters displayed for Norway spruce are common values at around 12 % moisture content [11]. Values are also displayed for strength class C24. The values displayed are characteristic stiffness values for CLT elements with strength class C24, based on the stiffness properties of the lamellas [1].

Table 2.1: Properties for different wood species.

Parameter	Norway spruce	C24	Birch [12]	Beech
E_L [MPa]	13500 – 16700	11000	15000	12306 [13]
E_R [MPa]	700 – 900	370	650	2280 [14]
E_T [MPa]	400 – 650	370	650	1160 [14]
G_{LR} [MPa]	620 – 720	690	850	–
G_{LT} [MPa]	500 – 850	690	850	–
G_{RT} [MPa]	29.0 – 39.0	50	175	470 [14]
ν_{LR}	0.018 – 0.030	–	–	–
ν_{LT}	0.013 – 0.021	–	–	–
ν_{RT}	0.24 – 0.33	–	–	–

2.1.3 Shear stiffness properties

Rolling shear is the shear stress leading to shear strain in a plane perpendicular to the grain direction [15]. The rolling shear strength and stiffness is often significantly lower than the shear strength parallel to grain [1]. See Figure 2.2 for the definition of the three different shear moduli for an orthotropic material with L , R and T as the main directions.

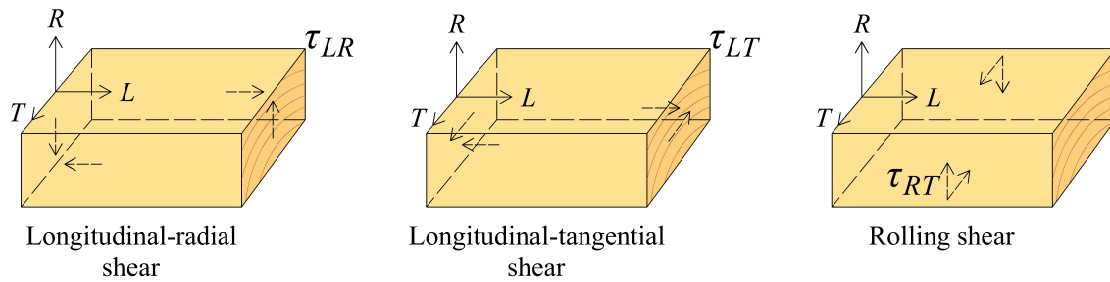


Figure 2.2: Illustration of shear loading in an orthotropic material with L , R and T as the main directions.

Since CLT is built up by layers with their grain directions in two different directions (see Section 2.2), the transverse layers will be subjected to rolling shear when they are placed perpendicular to the main span. And since the rolling shear modulus typically is low for timber used in CLT, this is of significant importance for both ultimate limit state design and serviceability limit state design for CLT [10].

The properties of the effective rolling shear modulus is influenced by a number of factors. The effective rolling shear modulus is the rolling shear modulus of a transverse layer, when viewing a CLT-beams' cross section. Previous research indicates that the aspect ratio of the width and the thickness of the lamellas and the annual ring orientation are the two of the most influential parameters [16]. The orientation of the annual rings is dependent on the sawing pattern of the board. A board can be sawn in multiple ways which gives different angles to the annual rings in relation to the pith, see Figure 2.3. The reason why this parameter is of such influence is the stiffness ratio of the radial and tangential plane [10] and in turn the stiffness ratio will affect the rolling shear.

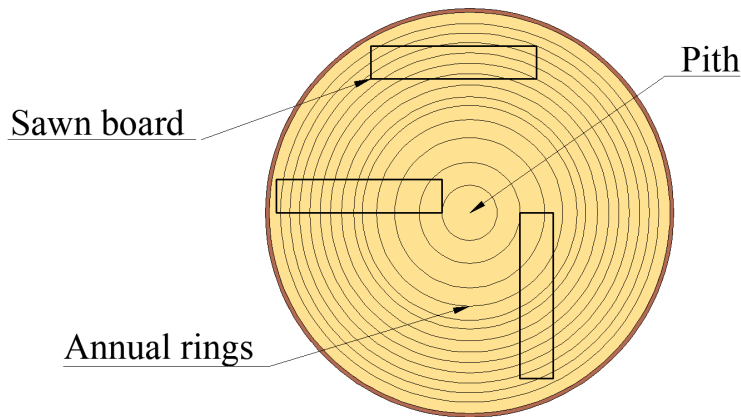


Figure 2.3: Annual ring orientation depending on the sawing pattern.

2.2 Cross Laminated Timber

CLT is an engineered timber product that consists of at least three layers of timber lamellas. The lamellas in each layer are placed side-by-side and glued together with the adjacent layers. The boards can also be glued together by the edges. Each layer is placed with the fiber direction of the boards perpendicular to the adjacent layer, giving the name cross laminated.

Common number of layers are three, five and seven. For a beam or slab the uneven number is used to keep the outermost layers parallel to the main span direction, to utilize the material in the most favourable way [1]. This is due to the fact that the longitudinal stiffness is the highest. Since the boards are cross laminated load carrying in two direction is made possible, making CLT have a plate-like behaviour. The plate-like element is favorable since it can be used as complete wall or floor element [17]. CLT can therefore be used as a compliment or replacement to concrete in some areas of construction. This has grown significant importance in recent years since timber products have a lower environmental impact compared to concrete [18].

When it comes to describing the loading directions of CLT, it differs from concrete and steel. This is because the orthogonal behaviour of the timber lamellas that CLT is made of. CLT has three global axes that are defined in [1] as (see Figure 2.4)

- the x -axis is parallel to the grain direction of the outermost layers.
- the y -axis is perpendicular to the grain direction of the outermost layers.
- the z -axis is perpendicular to the xy -plane.

Local axes for longitudinal and transverse lamellas are described with the three main directions of timber L , R and T , see Figure 2.4.

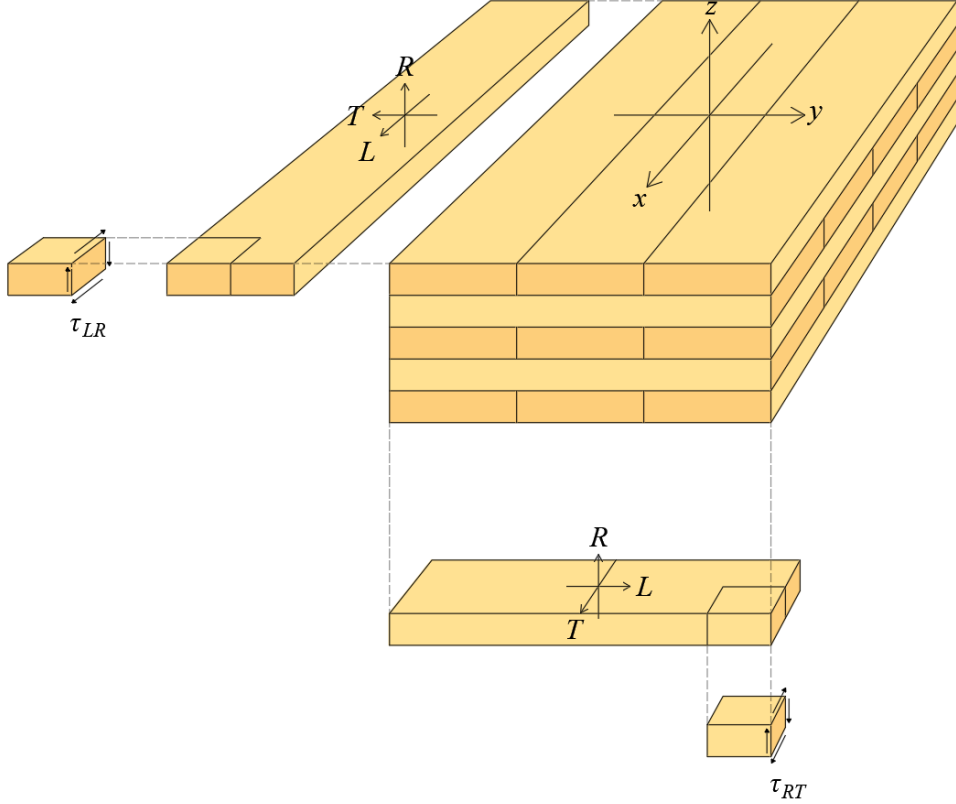


Figure 2.4: Main- and local axes of a CLT element.

2.3 Beam theory

For the evaluation of the testing method described in EN 16351 Annex C [5], the first step was to determine the deflection using Timoshenko beam theory which the test is based on. The deflection was also analysed with Bernoulli Euler theory. For Bernoulli Euler theory the deflection is only dependent on deformation due to bending whereas Timoshenko theory considers deformation due to both bending and shear (for the total deflection) [19].

For Bernoulli Euler theory the different properties of the longitudinal and transverse layers are considered with an effective moment of inertia. The effective moment of inertia is calculated according to the Gamma-method, further described in Section 2.3.1. For Timoshenko theory only the longitudinal layers contribute to the moment of inertia. This is described as the net moment of inertia, see Section 2.3.2.

The modulus of elasticity for the layers perpendicular to the main span direction are assumed to be zero when applying both theories on CLT. This is due the stiffness properties being significantly different for the three main directions. The difference in stiffness between the longitudinal (E_L) and the radial (E_R) or tangential (E_T) direction is considered large enough to assume zero stiffness in the radial and tangential direction i.e. $E_R = E_T = 0$.

2.3.1 Bernoulli Euler beam theory and Gamma-method

The Bernoulli Euler theory is based on the following three primary assumptions

- cross-sections are assumed to be rigid surfaces during deformation
- plane sections remain plane and normal to the beam axis during deformation
- the rotation angles (slope of the displacement) are small

Based on these three assumptions the rotation of the cross-section θ is equal to the slope of the beam w' , which means that the shear strains are not considered. Even though the shear strains are zero for calculations they are not zero in reality. A simplified way to assess the contribution from shear is to replace the net moment of inertia I_{net} with the effective moment of inertia I_{ef} calculated with the Gamma-method [1].

The Gamma-method is derived from the Mechanically joint beam-method described in Eurocode 5, Annex C, [1]. The method can be applied to CLT by viewing each longitudinal layer as an individual beam and introducing connection factors that account for the shear deformations of the transverse layers [20]. The factors are called Gamma-factors ($\gamma \leq 1$) and reduce the second part of Steiner's theorem for the longitudinal layers [1], see Equations 2.12 and 2.13.

Every layer is numbered from bottom to top, see Figure 2.5 for a five layered CLT slab.

$$I = \sum_{i=1}^n \frac{bt_i^3}{12} + bt_i a_i^2 \quad i = 1, 3, 5 \quad (2.12)$$

$$I_{ef} = \sum_{i=1}^n \frac{bt_i^3}{12} + \gamma bt_i a_i^2 \quad i = 1, 3, 5 \quad (2.13)$$

The Gamma-factors for a five layered element are calculated as

$$\gamma_1 = \left(1 + \frac{\pi^2 E_L t_1}{l_{ref}^2} \frac{t_2}{G_{RT}} \right)^{-1} \quad (2.14)$$

$$\gamma_3 = 1 \quad (2.15)$$

$$\gamma_5 = \left(1 + \frac{\pi^2 E_L t_5}{l_{ref}^2} \frac{t_4}{G_{RT}} \right)^{-1} \quad (2.16)$$

As can be seen in Equations 2.14 and 2.16 the Gamma-factors are dependent on the reference length (l_{ref}) of the beam, the thicknesses of the lamellas (t_i), the stiffness

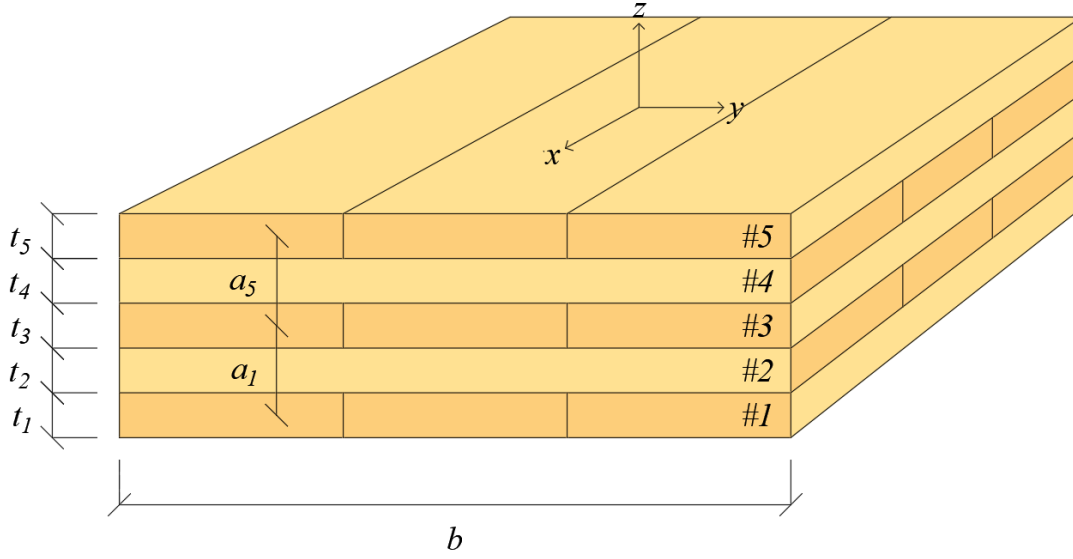


Figure 2.5: Numbering of the layers for a five layered CLT slab.

of the longitudinal layers (E_L) and the rolling shear stiffness (G_{RT}). The value (γ_3) for the mid layer is equal to 1 due to symmetry. For a simply supported beam, which is the case in this report, the reference length is equal to the span length [1]. The Gamma-factors also depend on the load, and the expressions 2.14 and 2.16 are derived for the case of distributed load. This influence is not taken into account here.

For CLT elements with seven or nine layers a more complicated version of the Gamma-method must be applied [1]. For this report the analysis is limited to five layer elements.

The effective moment of inertia calculated with the Gamma-method is then implemented in the equations used to describe the deformations according to the Bernoulli Euler theory. For the four-point bending set-up described in Section 2.4, the total deformation of the beam can be described by superposition of two point loads at arbitrary placement along the beam. The load case is shown in Figure 2.6. The total deflection at the mid-span of the beam is calculated according to Equation 2.17.

$$w = \frac{Pa(3L^2 - 4a^2)}{24E_L I_{ef}} \quad (2.17)$$

Thus from the expressions 2.17 and 2.13, it is clear that the transverse layers are assumed not to contribute to the stiffness.

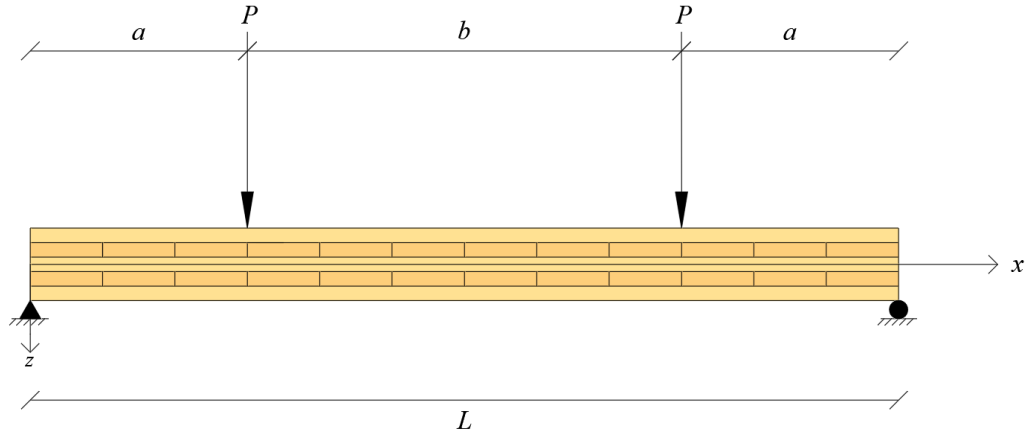


Figure 2.6: Load case with the arbitrary distances a and b .

2.3.2 Timoshenko theory

Timoshenko beam theory is similar to Bernoulli Euler as the assumption that plane sections remain plane during deformation applies for both theories. The main difference between the two theories is that for Timoshenko theory shear strains are considered [19]. Shear strains cause shear deformation, meaning that the total deformation is dependent on both bending and shear. The shear strains can be derived as the difference between the rotation and the slope of the beam ($\theta - w'$). Since the shear stiffness perpendicular to grain (rolling shear stiffness) is low for timber commonly used in CLT, the transverse layers of a CLT slab are prone to shear deformations, see Section 2.1.3. Timoshenko theory is therefore of significant interest when analysing the deformation of CLT.

When applying Timoshenko theory to CLT, it is typically assumed that only the longitudinal layers contribute to the moment of inertia, which is based on the assumption of zero normal stiffness in the transverse layers. This is called the net moment of inertia and is for a five layered element determined according to

$$I_{net} = \frac{bt_1^3}{12} + bt_1a_1^2 + \frac{bt_3^3}{12} + \frac{bt_5^3}{12} + bt_5a_5^2 \quad (2.18)$$

The deflection caused by bending can be determined the same way as for Bernoulli Euler in Section 2.3.1, by replacing the effective moment of inertia (I_{ef}) with the net moment of inertia (I_{net}). Since Timoshenko considers shear strains, the total deflection is dependent on both bending and shear. The shear deflection caused by constant shear force (which is the case for point loads) can be derived to

$$(w' - \theta)x = \frac{V}{D_{GA}}x \quad (2.19)$$

where x is any position along the beam where the shear force V is constant. $(w' - \theta)$ is the shear angle which is the difference between the slope of the beam w' and the rotation of the beam θ . D_{GA} is the cross section shear stiffness, given by the sum of the layer area multiplied with the shear modulus for every layer according to

$$D_{GA} = \kappa \sum_{i=1}^n A_i G_i \quad (2.20)$$

where κ is a shear correction factor. κ is used to reduce the shear stiffness over the entire cross section, to account for the overestimation of the stiffness due to the assumption that plane sections remain plane. For homogeneous and rectangular cross sections the shear correction factor is set to $5/6$, for CLT-elements it can be determined according to [1]

$$\kappa = \frac{(\sum (EI + EAa^2))^2}{\sum G_i b t_i \int_h \frac{S^2(z) E^2(z)}{G(z) b(z)} dz} \quad (2.21)$$

where S is the static moment, E is the modulus of elasticity, I is the moment of inertia, A is the cross section area, G_i is the shear modulus for each layer, b is the width of the layers, t_i is the thickness for each layer and a is the distance between the center of gravity for each layer and the center of gravity for the entire cross section.

The total deflection of the mid-span for the loading and support conditions according to Figure 2.6 can then be derived according to

$$w = \frac{Pa(3L^2 - 4a^2)}{24E_L I_{net}} + \frac{P}{D_{GA}} a \quad (2.22)$$

2.4 Testing method

The testing method evaluated in this thesis is a four-point bending test for determining the shear strength and stiffness properties of CLT. The load configuration and test set-up can be found in Annex C Figure C.5 in the European standard EN-16351 [5] and is shown in Figure 2.7. The span length is set to twelve times the height of the beam, with the grain of the outermost layers parallel to the span. The two loads are placed three times the height from the supports on each side [5]. The distance a in Figure 2.7 can also be change to six times the height from the supports which is described in EN-16351 [5]. This can be done if the aim is to only determine the shear strength.

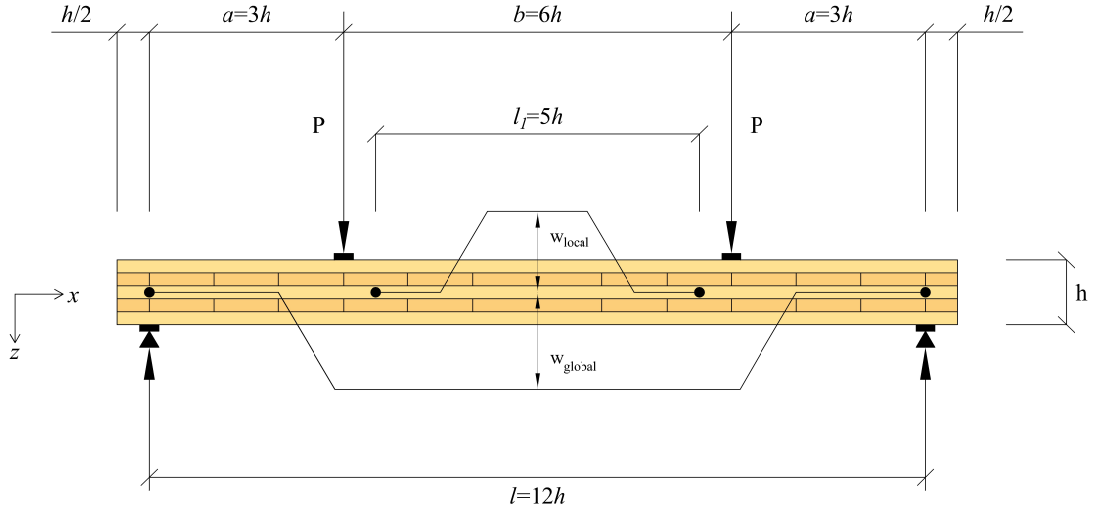


Figure 2.7: The four-point bending test set-up.

The deflection is measured as both global (w_{global}) and local deflection (w_{local}) as shown in Figure 2.7. The measurement points are placed at the mid-height of the beam. Both the global and local deflection shall be measured continuously and evaluated with results between 10% and 40% of the maximum load (P_{max}) [21]. The maximum load is obtained just before failure. The failure modes analysed are bending failure, longitudinal shear failure and rolling shear failure. Since no laboratory test were performed for this project the maximum load was instead based on beam theory and was determined by analysing the design verification of bending and shear stresses described in the CLT Handbook [1] as

$$\sigma_{m,x} = \frac{M_y}{W_{x,net}} \leq f_m \quad (2.23)$$

$$\tau_{v,xz} = \frac{S_{x,v} V_{xz}}{I_{x,net} b} \leq f_v \quad (2.24)$$

$$\tau_{Rv,xz} = \frac{S_{x,R} V_{xz}}{I_{x,net} b} \leq f_{Rv} \quad (2.25)$$

The moment and shear force diagram for the load case used in the test set up can be derived according to Figure 2.8. The moment M_y and the shear force V_{xz} in Equations 2.23-2.25 represent the largest value of moment and shear force diagram respectively. f_m is the bending strength, f_v is the longitudinal shear strength and f_{Rv} is the rolling shear strength. $W_{x,net}$ is the net moment of resistance and determined according to

$$W_{x,net} = \frac{2I_{x,net}}{h} \quad (2.26)$$

$S_{x,v}$ and $S_{x,R}$ are net static moments which are used to determine the maximum longitudinal- and rolling shear stress respectively. The numbering of the layers are starting from the bottom and up according to Figure 2.5. For a five layered CLT-beam the net static moments are determined according to

$$S_{x,v} = bt_5 \left(\frac{t_3}{2} + t_4 + \frac{t_5}{2} \right) + b \frac{t_3}{2} \frac{t_3}{4} \quad (2.27)$$

$$S_{x,R} = bt_5 \left(\frac{t_3}{2} + t_4 + \frac{t_5}{2} \right) \quad (2.28)$$

Since timber is an orthotropic material the stiffness properties vary significantly between the three main directions. The difference in stiffness between the longitudinal (E_L) and the radial (E_R) or tangential (E_T) direction is considered large enough to assume zero stiffness in the radial and tangential direction i.e. $E_R = E_T = 0$. This assumption for CLT indicates that there can be no bending stresses in the transverse layers. The bending stress is therefore assumed to be linearly distributed over the longitudinal layers only, see Figure 2.9.

The shear stresses act in two different directions with respect to the material directions. The longitudinal layers are subjected to longitudinal shear and the transverse layers are subjected to rolling shear. The longitudinal shear strength is significantly higher than the rolling shear strength. Due to this, rolling shear failure is the most likely failure mode, even if the maximum shear stress is obtained at half the beam height in the mid longitudinal layer. The shear stress distribution is illustrated in Figure 2.9.

By rewriting Equation 2.23, 2.24 and 2.25 the maximum force can be derived according to

$$P_{max,m} = \frac{W_{x,net} f_{mk}}{a} \quad (2.29)$$

$$P_{max,v} = \frac{f_v I_{x,net} b}{S_{x,v}} \quad (2.30)$$

$$P_{max,vR} = \frac{f_{Rv} I_{x,net} b}{S_{x,R}} \quad (2.31)$$

The lowest value from Equation 2.29, 2.30 and 2.31 will be regraded as the maximum load obtained before failure.

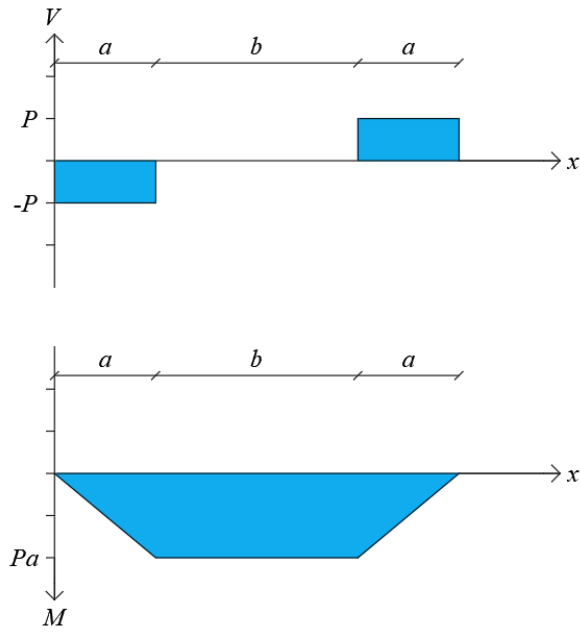


Figure 2.8: Shear- and moment diagram for the four-point bending test.

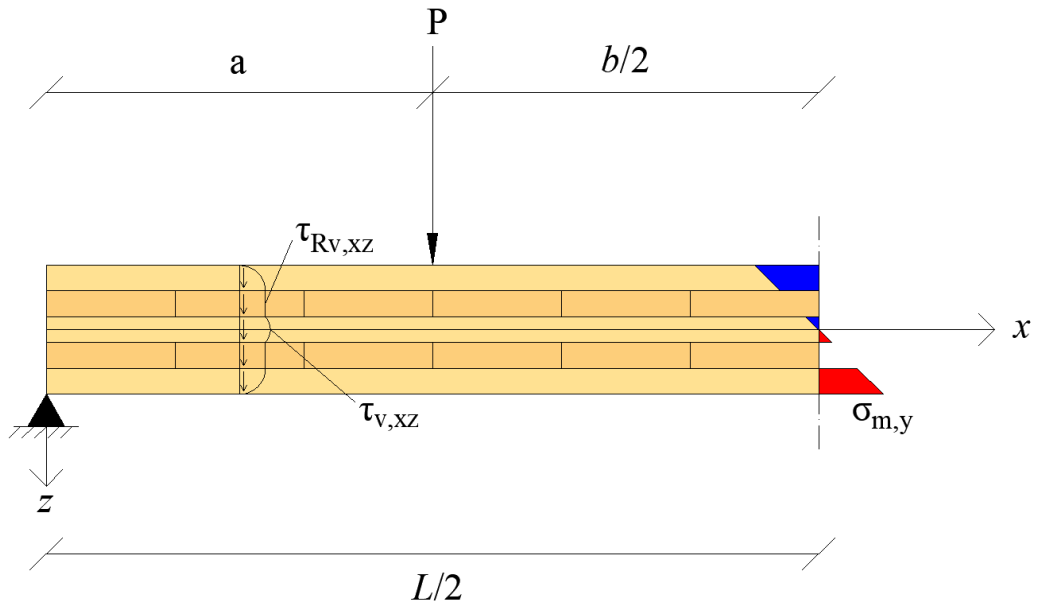


Figure 2.9: Sketch of half beam showing the bending stress distribution at mid-span (constant moment) and the shear stress distribution between support and load (constant shear force).

Further conditions for the test set-up described in [5] include

- Every board of the CLT element shall have the same strength class.
- The width of the tested CLT element shall be at least 600 mm.
- The tested CLT element shall consist of five layers.
- Tests shall have the outermost layers parallel to the span.

The standard also states that the ratio between the width w and the thickness t of the lamellas shall be at least four ($w/t \geq 4$). The ratio will be used as one of the variable parameters when evaluating the test with a parametric study further described in Section 3.3.1.

The standard also mentions the shear correction factor κ which is further discussed in Section 2.3.2. The correction factor is determined by the dimensions and stiffness properties of the lamellas, but can according to the preconditions described in [5] be set to 0.25 regardless of the size of the lamellas. The effect of the magnitude of κ was part of the evaluation as this could affect the results significantly.

The test specimens shall be made from spruce or pine, which are both softwood species. When evaluating the test the mean value of the shear stiffness in the longitudinal-radial direction is assumed to be 650 MPa [5]. This assumption is essential when determining the shear stiffness properties, further discussed in Section 2.4.1.

2.4.1 Evaluation of test results

To evaluate the results of the four-point bending, there are a set of equations given in EN-16351 [5] for the properties being analyzed. The evaluations are based on the measured global and local deflections for loading between 10% and 40% of the maximum load. The relation between the deflections and load found from tests can be approximated as a linear relation according to Figure 2.10.

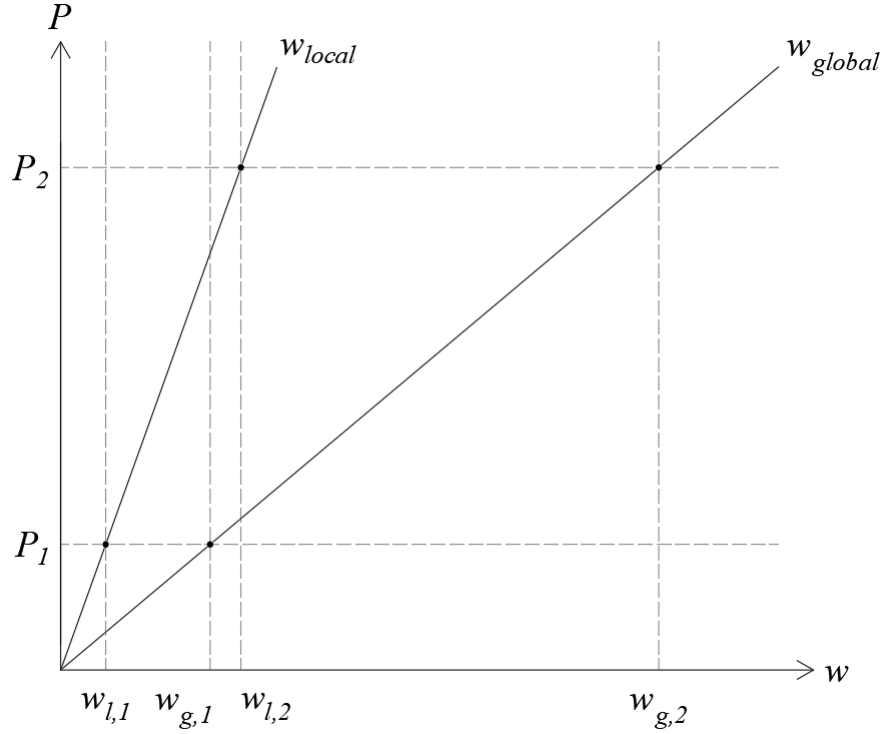


Figure 2.10: Linear relation between deformation and load.

The relation between the load and the local deflection can be used to determine the local bending stiffness $(EI)_{local,net}$. The local deflection is measured between the loads at the distance l_1 see Figure 2.7. The moment is along l_1 is constant and the shear force is zero. The local bending stiffness $(EI)_{local,net}$ represents the longitudinal stiffness E_L times the net moment of inertia I_{net} . It can be derived from the load case of a simply supported beam with constant moment with beam theory according to

$$w = \frac{Ml_1^2}{8(EI)_{local,net}} \quad (2.32)$$

where for the test set-up in Figure 2.7

$$M = aP \quad (2.33)$$

and the local bending stiffness can then be determined from the linear relation $\Delta P/\Delta w_l$ as

$$(EI)_{local,net} = \frac{al_1^2 \Delta P}{8 \Delta w_l} = \frac{al_1^2 (P_2 - P_1)}{8 (w_{l,2} - w_{l,1})} \quad (2.34)$$

The local bending stiffness is determined by the deflection dependent on only bending deformations. The deflection of the entire beam (w_{global}) is dependent on both bending

and shear. An *apparent* bending stiffness can be derived based on the global deflection. This is derived from the deflection at mid-span (see Equation 2.22), by assuming infinite shear stiffness D_{GA} (equal to Bernoulli-Euler theory) according to

$$w_g = \frac{Pa(3L^2 - 4a^3)}{24(EI)_{app,net}} \quad (2.35)$$

and the apparent bending stiffness can then be determined from the linear relation $\Delta P/\Delta w_g$ as

$$(EI)_{app,net} = \frac{a(3L^2 - 4a^2)}{24} \frac{\Delta P}{\Delta w_g} = \frac{a(3L^2 - 4a^2)}{24} \frac{(P_2 - P_1)}{(w_{g,2} - w_{g,1})} \quad (2.36)$$

The shear stiffness for the entire cross section D_{GA} of the specimen is determined with a relation between the local and apparent bending stiffness according to Equation 2.37. The difference between the global deflection w_g , which is dependent on both bending and shear, and the local deflection w_l , which is only dependent on bending, gives information about the shear deflections.

$$D_{GA} = \frac{24(EI)_{local,net}(EI)_{app,net}}{(3L^2 - 4a^2)((EI)_{local,net} - (EI)_{app,net})} \quad (2.37)$$

The term D_{GA} represent the total shear stiffness of the entire cross section and is the sum of the shear modulus for each layer multiplied with the corresponding layer area.

The conditions previously mentioned in Section 2.4 state the assumption of 650 MPa as the shear modulus of the longitudinal layers (longitudinal-radial shear G_{LR}). By using this assumption the shear modulus of the transverse layers can be determined by comparing Equation 2.37 and the total shear stiffness as described in Equation 2.38. This means that by assuming the longitudinal-radial shear modulus G_{LR} the rolling shear modulus G_{RT} can be determined based on measurements, see Equation 2.39.

$$D_{GA} = \kappa \sum_{i=1}^n A_i G_i = \kappa bt (3G_{LR} + 2G_{RT}) \quad (2.38)$$

$$G_{RT} = \frac{1}{2} \left(\frac{D_{GA}}{\kappa bt} - 3G_{LR} \right) \quad (2.39)$$

κ is a shear correction factor which is further discussed in Section 2.3.2. The shear correction factor κ is determined by the dimensions and stiffness properties of the lamellas, but can according to the preconditions described in [5] be set to 0.25 regardless of the size of the lamellas. The effect of the magnitude of κ was part of the evaluation as this could effect the results significantly.

In order to determine the rolling shear stiffness G_{RT} the testing method is restricted by assumption in Equation 2.39. As for most material properties for timber both longitudinal-radial and rolling shear moduli display uncertainties when being measured. The uncertainty of the input arises questions of the certainty of the output. A thorough evaluation of the input assumptions and the sensitivity of the input parameters of Equation 2.39 can be seen as a cornerstone for this dissertation.

2.5 Finite element method

The finite element method (FEM) is a numerical method used to solve partial differential equations, by dividing a larger system into smaller parts called finite elements. Each element is in turn described by a set of nodes. A node marks a single point and the behaviour of each node is described by a set of degrees of freedom *dof*, which for example describes how the node moves or rotates in each direction. The properties of each element are described by an element stiffness matrix \mathbf{K}^e and an element load vector \mathbf{f}^e . The local stiffness matrix and local load vector are assembled together for every element to describe the entire system. The displacements of each node are obtained by solving the global equation $\mathbf{K}\mathbf{a} = \mathbf{f}$, where \mathbf{a} describes the displacements of every *dof* in each node.

When analysing a beam with the use of FEM the most simple method is to divide the beam into line-elements (see Figure 2.11) and apply beam theory. This can be done for both Bernoulli Euler and Timoshenko theory with the use of the finite element toolbox *Calfem*, by applying nodes and line-elements to the center line of a beam. This method gives exact solutions of the displacements for the nodes within the assumptions for the analysed beam theory. This is further discussed in Section 3.1.1.

Approximate solutions can be analysed for two- and three dimensional bodies with FE software programs such as Abaqus. For 2D-analysis the body analysed is divided into elements and nodes in two directions which mark the body's plane. This is illustrated for a CLT-beam in Figure 2.11 where x and y are the two directions which make up an xy -plane. The nodes are only expressed in this plane. To represent the width of a beam an out-of-plane thickness can be added as an input. 2D-analysis is suitable when displacements occur in the same directions as the nodes and elements are expressed in and response is constant in the out-of-plane direction i.e. plane stress or plane strain. This is often the case for a bending tests, since the load is applied in an in-plane direction.

For 3D-analysis, the body analysed is divided into nodes and elements in three directions. This is illustrated for a CLT-beam in Figure 2.11 with the three directions x , y and z . This means that the nodes are not just expressed in one plane, but are also expressed for the width and the volume of the body. The nodes can theoretically represent every point of the entire analysed body if the elements are infinitely small. The elements are however finite which means that the solutions will be approximate. The size of the elements is further discussed in Section 3.2.1.

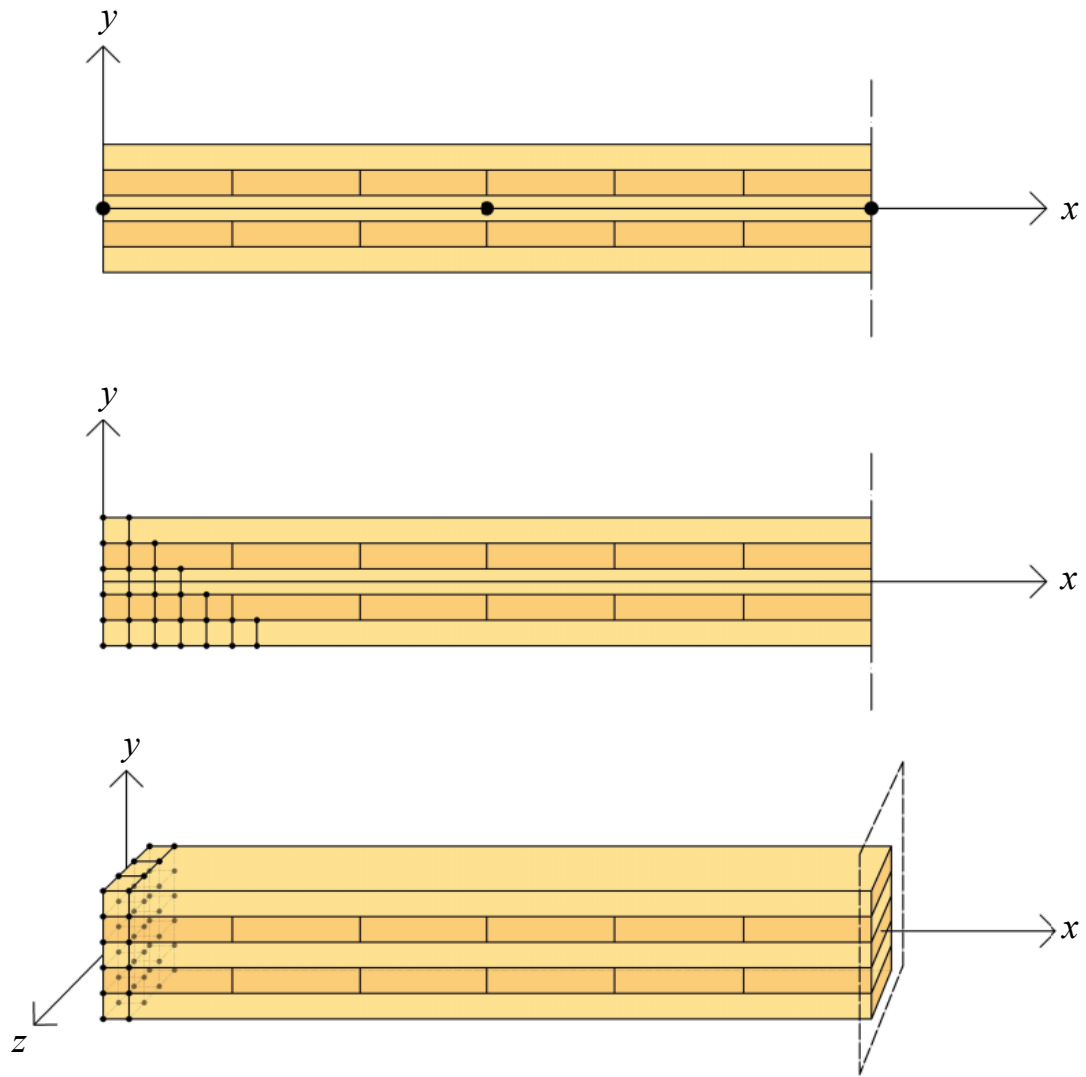


Figure 2.11: Line-elements (top), 2D-elements (middle) and 3D-elements (bottom).

3 Method

3.1 Deformation calculations

The deformation obtained from the four-point bending described in Section 2.4 was calculated both according to Bernoulli Euler theory with the use of the Gamma-method and Timoshenko beam theory. The deformation was calculated at mid-span of the beam, where the deformation reaches its maximum value.

In order to easily change parameters, such as lamella size and timber properties the calculations were done with the use of Matlab. The calculations were also compared with the Matlab toolbox *Calfem* [22]. *Calfem* is a finite element toolbox and was used to calculate the deflections with the finite element method.

3.1.1 Calfem

Both Bernoulli Euler- and Timoshenko theory was analysed using *Calfem*. Due to symmetry at the mid-span, half of the element in Section 2.4 was analyzed. The part was divided into three elements and four nodes. The first node was located at the support, the second node had the same location as the point load, the third node was located at the reference point for measurement of the local deformation, and the fourth node was located at the symmetry line, see Figure 3.1. The first, third and fourth node were used to give exact deformation within beam theory. The second node was used to apply the point load. Boundary conditions were applied to set limitations for the dofs. The following assumptions were set for the boundary conditions when analysing half of the beam

- No deformation in the y -direction at the support.
- No deformation in the x -direction at mid-span due to symmetry.
- No rotation at mid-span due to maximum deflection.

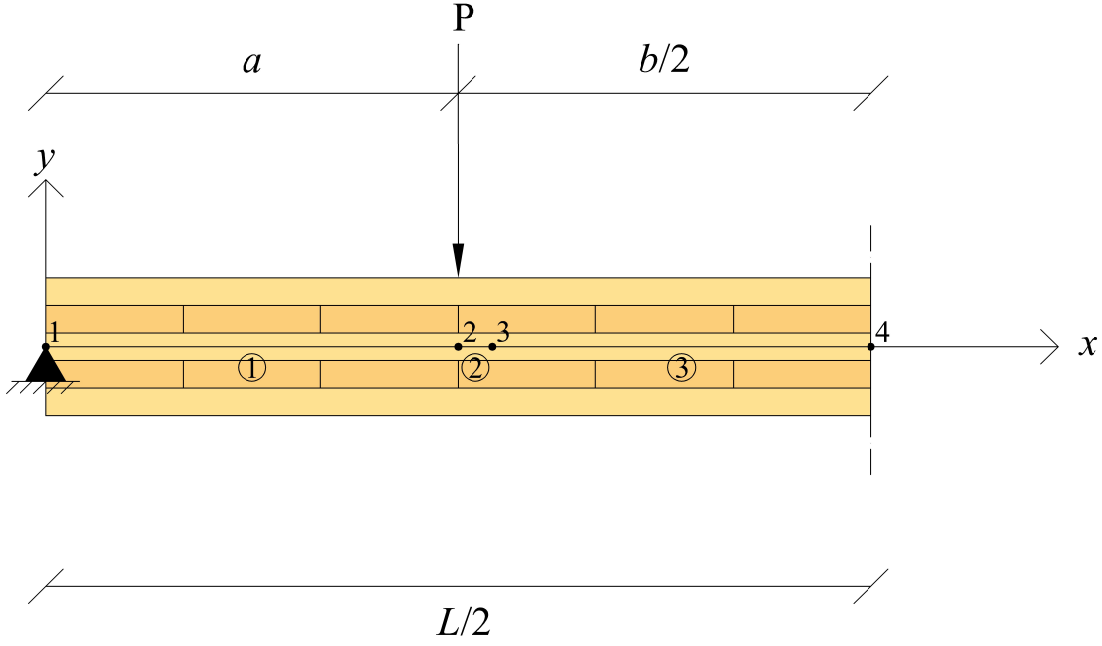


Figure 3.1: Half of the beam divided in to elements and nodes.

The Calfem function *beam2e* was used to compute the stiffness matrix for all three elements according to Bernoulli Euler theory, considering the effective bending stiffness according to the Gamma-method. The input parameters for this function are the element node coordinates, element properties and the distributed loads which in this case was zero. The element properties needed for Bernoulli Euler theory are the MOE of the longitudinal layers (E_L), the cross section area (A_{net}) and the effective MOI (I_{ef}), expressed with the vector ep

$$ep = [E_L \quad A_{net} \quad I_{ef}] \quad (3.1)$$

A stiffness matrix was computed for all three elements and assembled with the function *assem*. The point load was applied by adding it to the fifth position of the global force vector \mathbf{f} . The fifth position represents the vertical displacement at the second node. The system of equations $\mathbf{K}\mathbf{a} = \mathbf{f}$ was solved with the function *solveq*. The displacements of the beam was obtained with the function *beam2s* with use of the solution of $\mathbf{K}\mathbf{a} = \mathbf{f}$. This gives an exact solution of the displacements within Bernoulli Euler beam theory.

A similar method was used for Timoshenko beam theory. The function *beam2t* was used to compute the stiffness matrix for all three elements. The input parameters for this function are the element node coordinates, element properties and the distributed loads which in this case were zero. The element properties needed for Timoshenko theory were expressed with the element properties vector as

$$ep = [E_L \quad G_{mean} \quad A_{net} \quad I_{net} \quad \kappa] \quad (3.2)$$

To account for the different shear moduli of the longitudinal and transverse layers a mean shear modulus for the entire cross section was determined according to

$$G_{mean} = \frac{(G_{LT}(t_1 + t_3 + t_5) + G_{RT}(t_2 + t_4))}{h} \quad (3.3)$$

A stiffness matrix was computed for all three elements and assembled with the function *assem*. The load vector \mathbf{f} was the same for both theories. The system of equations $\mathbf{Ka} = \mathbf{f}$ was solved with the function *solveq*. The displacements of the beam were obtained with the function *beam2ts* with use of the solution of $\mathbf{Ka} = \mathbf{f}$. This gives an exact solution of the displacements within Timoshenko beam theory. The deformation is illustrated with an example in Figure 3.2, showing the deformation at mid-span according to calculations according to both theories as described in Section 2.3.1 and 2.3.2. The illustration also shows the deflection for the three elements as the output of *beam2s* and *beam2ts*.

The load was represented by a vector with the first value representing 10 % of the maximum load and the second value representing 40 % of the maximum load. A *for - loop* was created to run the analysis for both loads. The measurement points described in Figure 2.7 were placed in node one, three, and four and represent the reference point for global deflections, the reference point for local deflections and the total deflections at mid-span. The deflections at the three measurements points for 10 % and 40 % of the maximum load were then used to evaluate the testing method according to the equations described in Section 2.4.1.

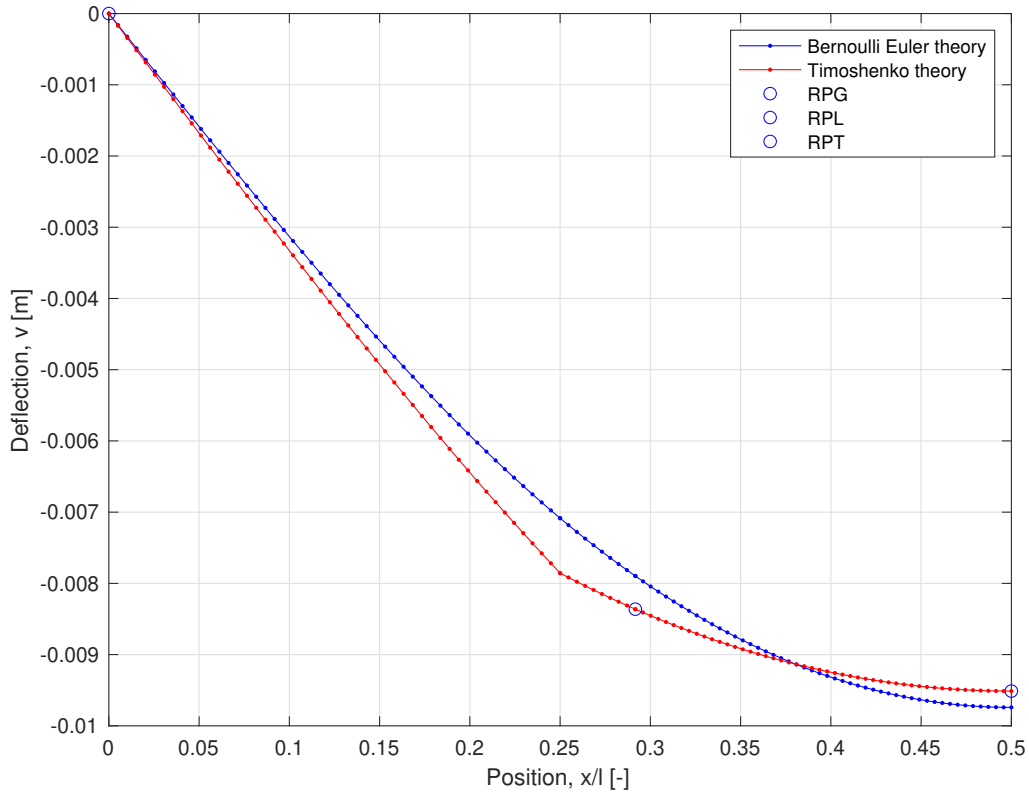


Figure 3.2: Example of deflection for a beam according to Bernoulli Euler and Timoshenko theory for $P_{max}=54.45$ kN. *RPG*, *RPL* and *RPT* are the measurement points for the deflections.

In addition to deflections the shear strains were also evaluated with the Calfem calculations. The shear strains are according to Timoshenko beam theory the difference between the rotation θ and the slope w'_T of the beam ($\theta - w'_T$). According to Bernoulli Euler beam theory the rotation θ of the beam is equal to the slope w'_{BE} . The shear strains can be determined to $(w'_{BE} - w'_T)$, if the net moment of inertia (I_{net}) is applied for both theories (i.e. if the Gamma-method is not applied).

The results from the Calfem calculations were used to compare with the results from the FE-models. As the Calfem calculations are based on beam theory they will yield exact solutions concerning the deflections and strains i.e. exact within the assumptions of the theories that the calculations are based on. And since the equations used to evaluate the testing method are also based on beam theory the results from Calfem were regarded as the correct answers.

3.2 Finite element modelling

The test-set up described in Section 2.4, is supposed to be used for laboratory testing of real CLT-elements. As this was not possible for this project the evaluation of the testing method was instead performed on finite element models (FE-models). The

FE-models were created to resemble real life laboratory tests as good as possible. The FE-software used for this purpose is called *Abaqus* and is suitable since it allows a high degree of altering properties. This attribute was effectively used in the parametric study described in Section 3.3.1.

3.2.1 2D-model

The test set-up in Section 2.4 was first modelled as a two-dimensional beam, see Figure 3.3. Since the load case is symmetric in the x -direction, only half of the beam was modelled. The first step was to model the longitudinal and transverse lamellas as two individual parts that were assembled into a CLT element.

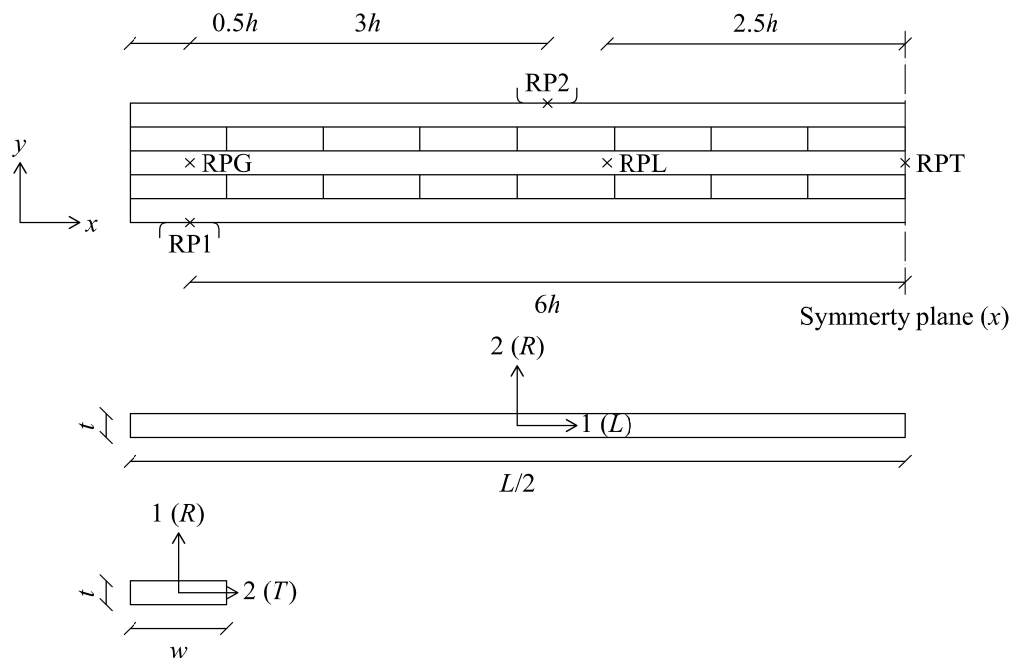


Figure 3.3: Sketch of the 2D-model.

Both the longitudinal part and the transverse part were given certain properties that represent timber lamellas. A material was created that represents the specific wood species used when performing the tests. For the longitudinal part the material was created with an elastic behaviour and the type *Lamina* which uses six of the twelve elastic constants that are described in Section 2.1.2, see Table 3.1.

Table 3.1: Material properties for the longitudinal and transverse lamellas.

Longitudinal boards	Transverse boards
$E_1 = E_L$	$E_1 = E_R$
$E_2 = E_R$	$E_2 = E_T$
$\nu_{12} = \nu_{LR}$	$\nu_{12} = \nu_{RT}$
$G_{12} = G_{LR}$	$G_{12} = G_{RT}$
$G_{13} = G_{LT}$	$G_{13} = G_{LR}$
$G_{23} = G_{RT}$	$G_{23} = G_{LT}$

The longitudinal part was assigned a material orientation to match the properties described in Table 3.1. A local Cartesian coordinate system with the first axis representing the longitudinal axis and the second axis representing the radial axis was created and assigned to the part. The transverse part was created with the same material type as the longitudinal part but with different material orientation. To analyse an assembly with different parts in Abaqus, all parts need to have the third axis in the same direction. To cope with this and to represent the 90° turn of the transverse lamellas a second material was created. The properties of the second material was chosen according to Table 3.1 material.

For the transverse part a cylindrical local Cartesian coordinate system was created to match the properties in Table 3.1. The cylindrical coordinate system was used to represent the annual ring orientation, with the first axis representing the radial axis and the second axis representing the tangential axis. The origin for the cylindrical coordinate system represents the pith of a tree and was scripted as a parameter to allow different annual ring orientation.

The parts were assembled with three layers of longitudinal parts and two layers with transverse parts, see Figure 3.3. The support and the load application surface were both modelled as analytical rigid surfaces. Both parts were modelled as a 50 mm long surface with *fillet* edges to avoid stress concentrations. The two parts were placed according to the test set-up in Section 2.4. The load application surface was rotated 180 relative to the support. The *reference point* for both the support and the load application surface were placed at the middle of the rigid surface, see Figure 3.3.

Interactions and contact conditions were added to the assembly. The constraints between the longitudinal and transverse layers were modelled as *ties*, with the surface of the longitudinal lamellas always being the *master surface*. The support and load application surface was given the constraint *Analytical Surface* and an *interaction property* between the two surfaces and the CLT element was added. The interaction property was assigned the following properties normal behaviour: "Hard" contact, tangential behaviour: *Penalty* with a coefficient of friction $\mu = 0.25$ and geometric properties with the out-of-plane thickness equal to beam width.

To perform a FE-analysis boundary conditions need to be set. The boundary conditions used for the 2D-model were set as:

- No vertical displacements at the support ($U_2=0$). Applied to the reference point for the support surface.
- Symmetry along the x-axis, meaning no horizontal displacements and no rotation along the z-axis ($U_1=0$, $UR_3=0$). Applied to the surfaces of the longitudinal boards at the symmetry line on the right edge of the model.

The load was applied to the reference point of the load application surface as a concentrated force. The magnitude of the force was determined according to Equation 2.31.

The model was divided into elements with the Abaqus module *mesh*. The element-type used for the 2D-analysis are called "CPS8 - eight node quadratic plane stress quadrilateral". The appropriate element-type was assigned after performing a convergence study, see Section 3.2.2. *CPS8* was chosen since it converged faster compared to other element-types. Full integration was chosen to avoid so called *hour-glass*-modes which is a spurious deformation mode where the deformation of an element doesn't match the deformation of the entire body.

3.2.2 Convergence study

A convergence study was done to see how refined the mesh had to be for the 2D-model. If a mesh is too coarse it might result in inaccurate results, the mesh therefore has to be refined until inaccuracies can be neglected. A mesh is considered to be converged when the difference in the result between two mesh refinements are considered small enough [23]. The degree of mesh refinement can also be connected to the time needed for Abaqus to process the analysis. The finer the mesh the longer the processing time will be. The mesh size chosen for this project was based on both the difference in result and the processing time. The aim was to find a mesh size with with a small enough result difference and reasonable processing time.

The convergence study for the 2D-model was done with two different element types, "CPS4 – four node bilinear plane stress quadrilateral" and "CPS8 – eight node bi-quadratic plane stress quadrilateral". Both element types were also tested with reduced integration, denoted as *CPS4R* and *CPS8R*. The study was performed on a 2D-modelled CLT-beam with homogeneous layers. The lamella thickness was set as 20 mm, giving the beam height 100 mm for a five layered beam. The assigned material properties were the same as for Norway spruce (see Table 2.1.2) and the load used was P_{max} , calculated according to Equation 2.31. The study was done by comparing the relative deflection at mid-span in relation to the number of elements in the height direction of the beam and the processing time. The results of the convergence study are illustrated as graphs in Figure 3.4.

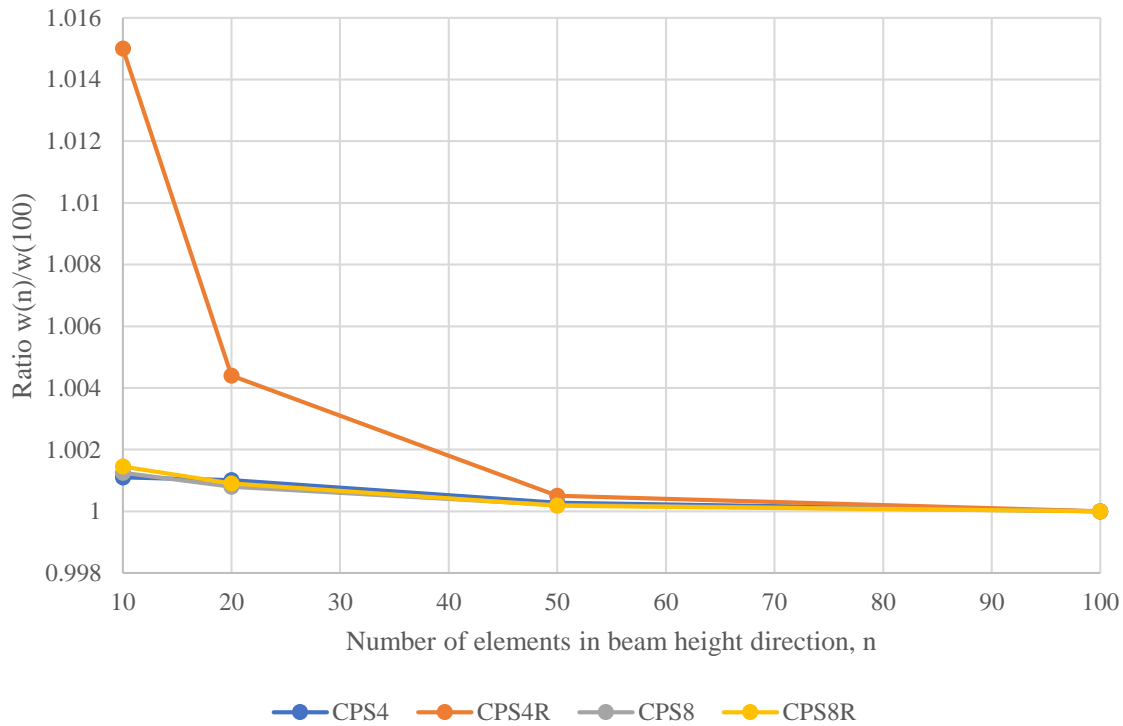


Figure 3.4: Convergence study.

The values in Figure 3.4 are normalized to the deflection at the mid-span at 100 elements in the beams height direction for each element type. The deflections for each element type are displayed in Table 3.2.

Table 3.2: Deflection at mid-span with 100 elements in the height direction of the beam for each element type. The load used is $P_{max} = 54.45$ kN.

Element type	Deflection at mid-span [mm]
CPS4	-9.36573
CPS4R	-9.36813
CPS8	-9.36664
CPS8R	-9.36674

The study showed that all element types studied converge almost equally fast except for CPS4R, this element type was therefore ruled out. The choice between the three other element types doesn't affect the results significantly. For this project the CPS8 element was chosen with 20 elements in the beam height direction. This mesh refinement was assumed to be good enough as the result difference between 20, 50 and 100 elements in the beam height direction was negligible small. The processing time would though increase from 2.9 seconds to 11.5 and 53.3 seconds. This increase of processing time would be inconvenient for the parametric study.

3.3 Evaluation of FE-models

To evaluate the FE-models, comparisons were done by analysing equal beams with Abaqus and with CalfeM. The output results of interest from both methods were the vertical deflections at the three nodes coinciding with the measurement points showed in Figure 3.3. The deflections were measured and compared at 10% and 40 % of the maximum load. In CalfeM this was achieved by performing a for-loop with the load as the input argument. In Abaqus each time-step was set to 0.1 and linearly increasing up to 1. Since the load also increased linearly the time-steps of 0.1 and 0.4 were assumed to represent 10% and 40 % of the maximum load respectively. The relations of the global and local deflections were determined according to

$$w_g(P) = (w_{RPT}(0.4P) - w_{RPG}(0.4P)) - (w_{RPT}(0.1P) - w_{RPG}(0.1P)) \quad (3.4)$$

$$w_l(P) = (w_{RPT}(0.4P) - w_{RPL}(0.4P)) - (w_{RPT}(0.1P) - w_{RPL}(0.1P)) \quad (3.5)$$

where RPG, RPL and RPT are the three measurement points described in Figure 3.3. The results for each model were then used to determine the apparent bending stiffness $EI_{app,net}$ (Equation 2.36) and the local bending stiffness $EI_{loc,net}$ (Equation 2.34) which in turn were used to determine the shear stiffness for the entire cross section D_{GA} according to Equation 2.37. By comparing the shear stiffness for the entire cross section according to the measurements and Timoshenko beam theory the output rolling shear modulus can be determined according to

$$G_{RT,output} = \frac{1}{2} \left(\frac{D_{GA}}{\kappa bt} - 3G_{LR} \right) \quad (3.6)$$

The essential evaluation of the testing methods' capability of determining the rolling shear stiffness of a CLT-beam is based on this Equation. The accuracy of the results are evaluated by comparing the input rolling shear modulus $G_{RT,input}$ with the output rolling shear modulus $G_{RT,output}$, and where correct results should result in

$$G_{RT,input} = G_{RT,output} \quad (3.7)$$

The correct results will always be obtained with calculations according to beam theory. This is due to the fact that beam theory results in exact solutions (with beam theoretical assumptions considered) and that the equations used to evaluate the testing method are based on beam theory. To only evaluate the testing method with beam theory would therefore be pointless as this would always generate the same results. The exact results from beam theory calculations were instead used to evaluate the results from the FE-models. The FE-models were modelled to resemble real life beams, meaning that the results from the models were assumed to better represent results from real laboratory testings than beam theory would. By comparing the ex-

act solutions with the FE-results, factors affecting the outcome could be analysed and possible patterns in results could be detected.

Except from the input rolling shear modulus affecting the deflections which in turn affects the outcome of Equation 3.6, the value chosen for the shear correction factor κ also has significant impact on the outcome. The impact on the input arguments in Equation 3.6 had to be further analysed. This was done by performing a parametric study described in Section 3.3.1.

3.3.1 Parametric study

In order to evaluate the testing method described in Section 2.4 a parametric study was performed on the 2D-models. This was done by writing a python-script that generates multiple FE-models with different input parameters. A 2D-model was first created in Abaqus CAE according to the same method described in Section 3.2.1. Every sequence performed in Abaqus is recorded and written as python-code and saved in an *.rpy*-file. The file can then be opened with a text editor such as *Notepad++*. In the text editor a new script was created that imports data from the Abaqus model. The wanted sequence can be copied from the *.rpy*-file and added to the new script, where parameters can be added and altered. *for*-loops were used to create multiple models with different properties. The script was also constructed to export the wanted results to Excel-files. For this study the analysed results were the deflections of the nodes coinciding with the measurement points previously mentioned.

The beam was first modeled as a homogeneous beam, see Figure 3.5. To represent this all layers were modeled as longitudinal with the same stiffness properties. Typical properties of Norway spruce was used as reference when performing the analysis and values according to Table 3.3 were used.

Table 3.3: Properties of Norway spruce.

E_L [MPa]	E_R [MPa]	E_T [MPa]	ν_{LR}	G_{LR} [MPa]	G_{LT} [MPa]	G_{RT} [MPa]
11000	800	500	0.02	650	650	50

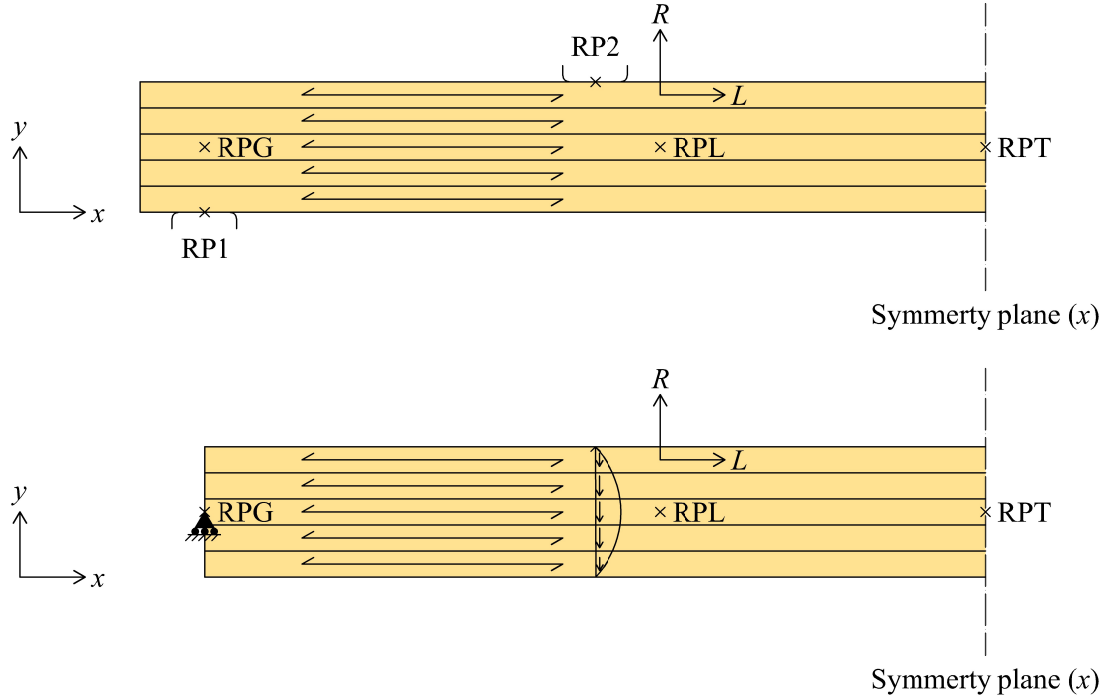


Figure 3.5: Sketch of homogeneous beam with loading conditions according to laboratory testing (top) and beam theory (bottom).

The interaction between the lamellas was modelled as ties both for the faces and the edges of the lamellas. The purpose of this was to perform tests on a beam that is not influenced by factors such as effective moment of inertia and varying shear correction factors etc. Since less factors influence a homogeneous beam the model was easier to compare to beam theory and to evaluate the equations used to determine the rolling shear modulus. The homogeneous beam was modelled with one longitudinal layer. This means that the longitudinal-tangential shear modulus G_{LT} applies for the entire cross-section. The shear correction factor κ was set as constantly $5/6$, which is the case for rectangular homogeneous beams. The output longitudinal-tangential shear modulus was analysed by decreasing the input longitudinal-tangential from 650 MPa to 50 MPa in steps of 50 MPa. The input and output was then compared in relation to each other according to

$$\frac{G_{LT,output}}{G_{LT,input}} \quad (3.8)$$

where the ratio of 1.0 means that the longitudinal-tangential shear modulus that was put into the FE-model is equal to the output. The output was determined according to

$$G_{LT,output} = \frac{6D_{GA}}{5hb} \quad (3.9)$$

where D_{GA} was evaluated using Equations 2.34 and 2.36.

Multiple factors influence the results of the determined output shear modulus in Equation 3.9. One factor that was noticed to deviate from the theoretical value was the local bending stiffness $(EI)_{local,net}$ which is determined according to

$$(EI)_{local,net} = \frac{al_1^2}{8} \frac{(P_2 - P_1)}{(w_{l,2} - w_{l,1})} \quad (3.10)$$

and represents the theoretical bending stiffness which is determined according to

$$E_L I_{net} \quad (3.11)$$

The length l_1 is the distance (between the point loads) over which the local deflections are measured and in a zone where the deformations are assumed to only be dependent on bending. When performing the analysis, the deviation between the measured (from the FE-models) and theoretical bending stiffness indicated that this wasn't the case and that shear deformations occurred between the loads as well. According to beam theory this shouldn't be the case as the shear force between the loads is zero. A possible improvement of the testing method could be to decrease the length l_1 towards the middle of the beam were the shear deformation should be less influential. To evaluate this, the length l_1 was decreased by steps of 25 mm on each side. The ratio between the measured bending stiffness in Equation 3.10 and the theoretical one in Equation 3.11 was then compared.

Since the equations that are used to determine the rolling shear modulus is based on Timoshenko beam theory, the beam was also modelled to resemble the theoretical load case, see Figure 3.5. The purpose of this was to evaluate the effects of differences between the testing set-up and the theoretical analysis. For the support the beam was modelled with a plane cross section rotating around a point at half the beam height. This was achieved by using the constraint *coupling* and setting the node at mid height as reference. Instead of applying a point load on the top surface of the beam, the load was applied to resemble the shear stress distribution. This was done by adding the load as a *surface shear traction* on the cross section at the same position in the x -direction where the point load was applied. A so called *analytical field* was used to distribute the shear stress to be equal to the theoretical stress distribution. The theoretical shear stress at the mid-height of the homogeneous beam was determined according to

$$\tau_{mid-height} = \frac{S_x V}{I_{net} b} = \frac{3P_{max}}{2bh} \quad \text{for } 0 < x < a \quad (3.12)$$

where V is the shear force of the beam which is equal to the point load P_{max} between the support and load and zero between the two point loads. The corresponding shear stress distribution for the homogeneous beam can be derived to

$$\tau(y) = \frac{-4\tau_{mid-height}}{h^2} (y^2 - hy), \quad 0 < y < h \quad (3.13)$$

where y represents the placement along the beam height h . The shear strain distribution over the height of the beam was determined according Equation 3.14. There is a contradiction in Timoshenko beam theory regarding Equations 3.13 and 3.14. For the derivation of the theory, the shear strains are assumed to be constant over the height of the beam. This, however, contradicts the equilibrium of the horizontal forces affecting the beam. In order to obtain equilibrium the shear stresses must vary over the height of the beam. This, in turn, affects the distribution of the shear strains. In this project the shear strains were analysed as varying over the height.

$$\gamma(y) = \frac{\tau(y)}{G}, \quad 0 < y < h \quad (3.14)$$

where G is the shear modulus for the corresponding layers of the beam. As the shear force is zero between the two point loads, also the shear stresses and the shear strains are zero according to beam theory.

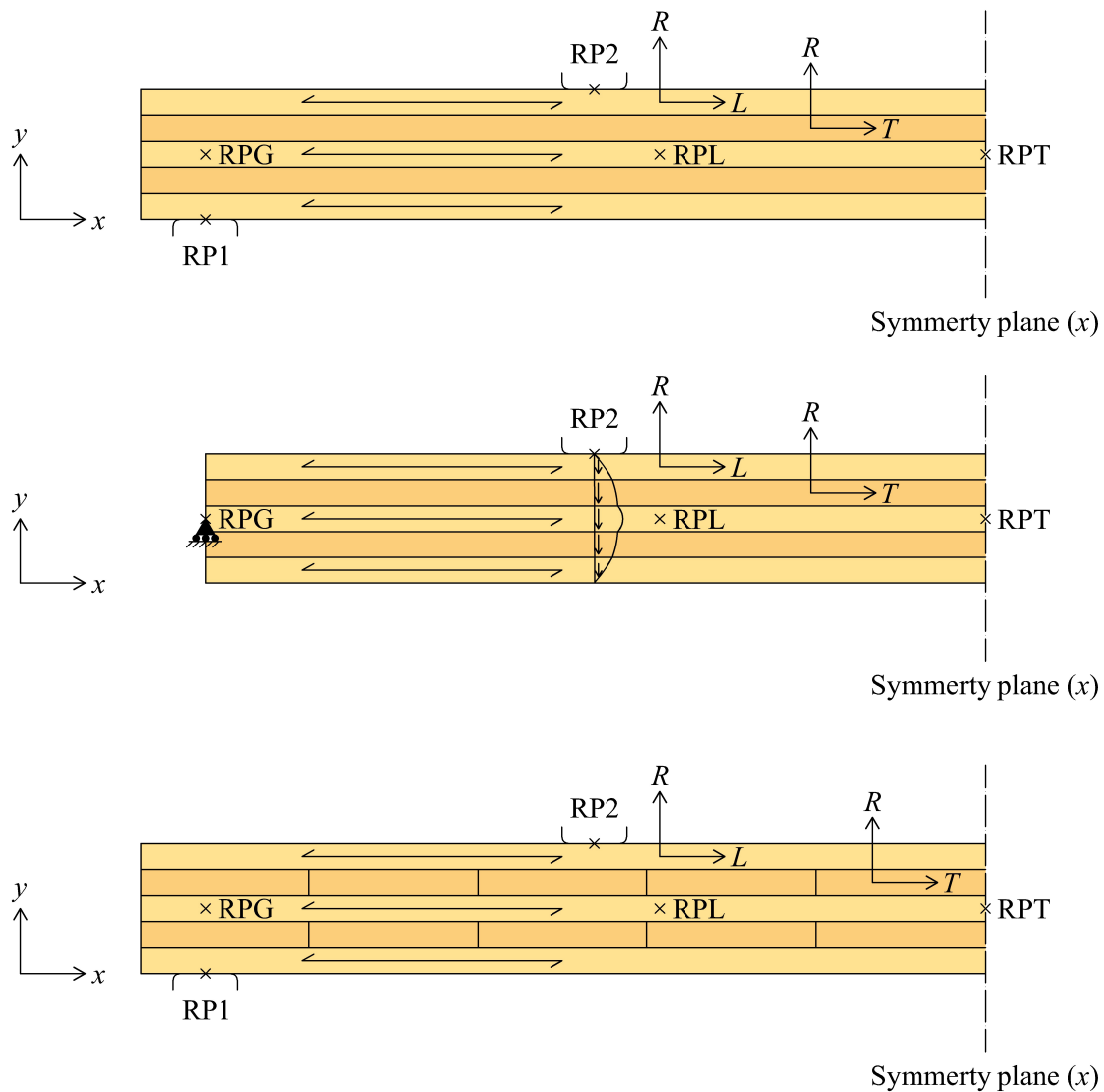


Figure 3.6: Sketch of CLT-beams with homogeneous layers and boundary conditions representing a laboratory test set-up (top) and Timoshenko theory (middle). Sketch of CLT-beam with transverse lamellas (bottom).

As a first step from the homogeneous beam towards a CLT-beam the transverse layers were implemented, but still seen as homogeneous within each layer i.e. the width of the lamella was equal to the beam length, see Figure 3.6. The transverse layers were assigned the material orientation described in Section 3.2.1. The CLT-beams were analysed in a similar fashion to the homogeneous beams with boundary conditions both representing a laboratory test set-up and Timoshenko beam theory, see Figure 3.6. The shear stress distribution over the height of a beam with the properties in Table 3.3, $P_{max}=54.45$ kN and $h=100$ mm can be derived to

$$\tau(y) = -6.75 \cdot 10^{-4} (y^2 - hy), \quad 0 < y < \frac{h}{5} \quad \& \quad \frac{4h}{5} < y < h \quad (3.15)$$

$$\tau(y) = -4.91 \cdot 10^{-5} (y^2 - hy + 1600) + 1.08, \quad \frac{h}{5} < y < \frac{2h}{5} \quad \& \quad \frac{3h}{5} < y < \frac{4h}{5} \quad (3.16)$$

$$\tau(y) = -6.75 \cdot 10^{-2} (y^2 - hy + 2400) + 1.12, \quad \frac{2h}{5} < y < \frac{3h}{5} \quad (3.17)$$

The shear strain distribution over the beam height was determined in the same fashion as for the homogeneous beams by dividing the shear stress $\tau(x)$ with the corresponding shear modulus G for each layer. For the CLT beams this means G_{LT} for the longitudinal layers and G_{RT} for the transverse layers.

The first parameter studied for the CLT-beams was the input rolling shear modulus which was first set as equal to the longitudinal-radial and the longitudinal-tangential shear modulus ($G_{RT} = G_{LR} = G_{LT}$) representing a constant shear stiffness over the entire cross section. Models with decreasing rolling shear modulus were created in a for-loop until the actual rolling shear modulus was reached. For Norway spruce the first model had a rolling shear modulus of 650 MPa, which then decreased by steps of 50 MPa for each new model until 50 MPa was reached. The output rolling shear modulus, was compared to the input rolling shear $G_{RT,input}$ (see Equation 3.8). The output rolling shear modulus was determined according to

$$G_{RT,output} = \frac{1}{2} \left(\frac{D_{GA}}{\kappa tb} - 3G_{LT} \right) \quad (3.18)$$

As described in the preconditions for this testing method the shear correction factor κ in Equation 3.18 can be altered and may be set as 0.25 for a beam with the rolling shear modulus $G_{RT}=50$ MPa. The theoretical value of κ for the beam with homogeneous layers and with the same rolling shear modulus was determined to 0.193 according to Equation 2.21. To analyse which impact the choice of the shear correction factor has on the output rolling shear modulus, Equation 3.18 was evaluated with different correction factors for the modelled beams.

To further evaluate the accuracy of the assumption that $\kappa=0.25$ for a beam with 50 MPa as the rolling shear modulus, the input rolling shear modulus was set to vary between 55 and 45 MPa. A deviation of ± 5 MPa was assumed to be relatively small and possible for a real beam.

The continuation from adding the transverse layers was to add varying width of the lamellas as displayed in Figure 3.6. No ties were modelled between adjacent lamellas. This was assumed to represent non edge glued lamellas. This was only analysed for the beams with boundary conditions representing a laboratory test set-up (BC type A). The ratio between the thickness and the width of the lamellas was expressed as the width w divided by the thickness t , see Figure 3.7. The width of the lamellas was

obtained by dividing the length of the model with the wanted number of transverse lamellas in order to only get complete lamellas. The width was limited to a minimum of four times the thickness i.e. $w/t \geq 4$, according to the conditions described in Section 2.4. The transverse layers were divided into eight, five and four lamellas which generated the following w/t -ratios for the analysed beam: 4.0625, 6.5 and 8.125.

The annual growth ring pattern was added to the models by assigning a cylindrical local coordinate system to the transverse lamellas. The center of the coordinate system represent the pith of a tree cross section. The location of the pith decides the pattern of the annual rings. A long distance between the lamellas and the pith gives more horizontal pattern of the annual rings whereas a short distance gives a more curved pattern. This is illustrated in Figure 3.7 where the bottom edge of the lamella is set as reference and the distance between the bottom edge and the pith is called c .

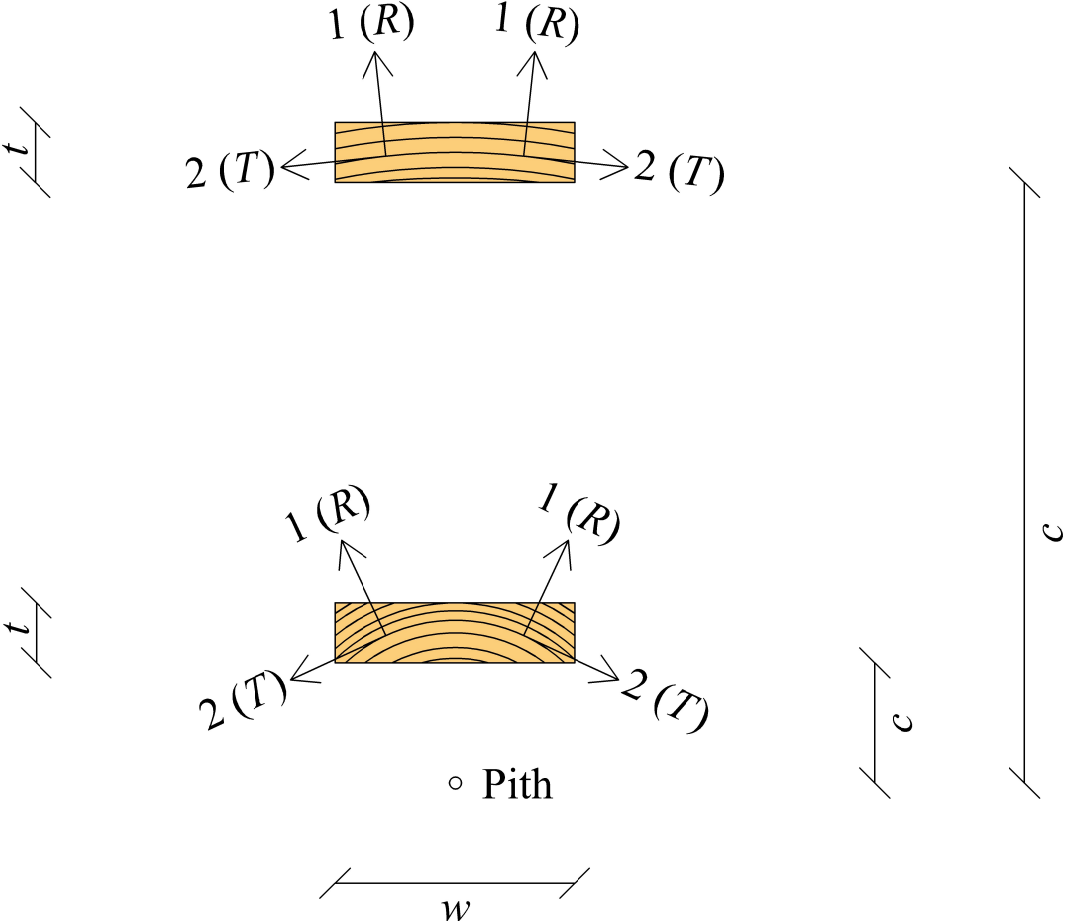


Figure 3.7: Sketch of transverse lamella showing the annual growth ring pattern and the distance c from the pith.

4 Results

When the 2D-model representing a laboratory test set-up of a CLT-beam (see Figure 3.6) was analysed, the results showed large deviations from what was expected. The output rolling shear modulus was for some values around seven times larger than the rolling shear modulus that was put into the FE-model. Before the parametric study where annual ring orientation and lamella thickness/width-ratio were evaluated, the factors leading to the inaccurate results had to be further investigated. To cope with this the model was instead simplified in several steps to resemble a theoretical Timoshenko beam. The purpose of this was to evaluate which factors and parameters that lead to the inaccuracy of the results.

The models were evaluated both with homogeneous layers and as CLT-beams with both longitudinal and transverse lamellas. Both beam types were modelled with boundary conditions representing a laboratory test set-up and Timoshenko beam theory as described in Chapter 3. Throughout this chapter the boundary conditions representing the laboratory test set-up are called *BC type A* for both the homogeneous- and CLT-beams. The boundary conditions representing Timoshenko beam theory are called *BC type B* and *BC type C* for the homogeneous- and CLT-beams respectively, see Figure 4.1 and 4.8. For BC type B and BC type C the loads were applied according to the theoretical shear stress distribution as described in Section 3.3.1. Figures 4.1 and 4.8 also displays the placement of the cross sections (*cross section 1* and *cross section 2*) where the shear strains were evaluated.

4.1 Evaluation of test

4.1.1 Homogeneous beams

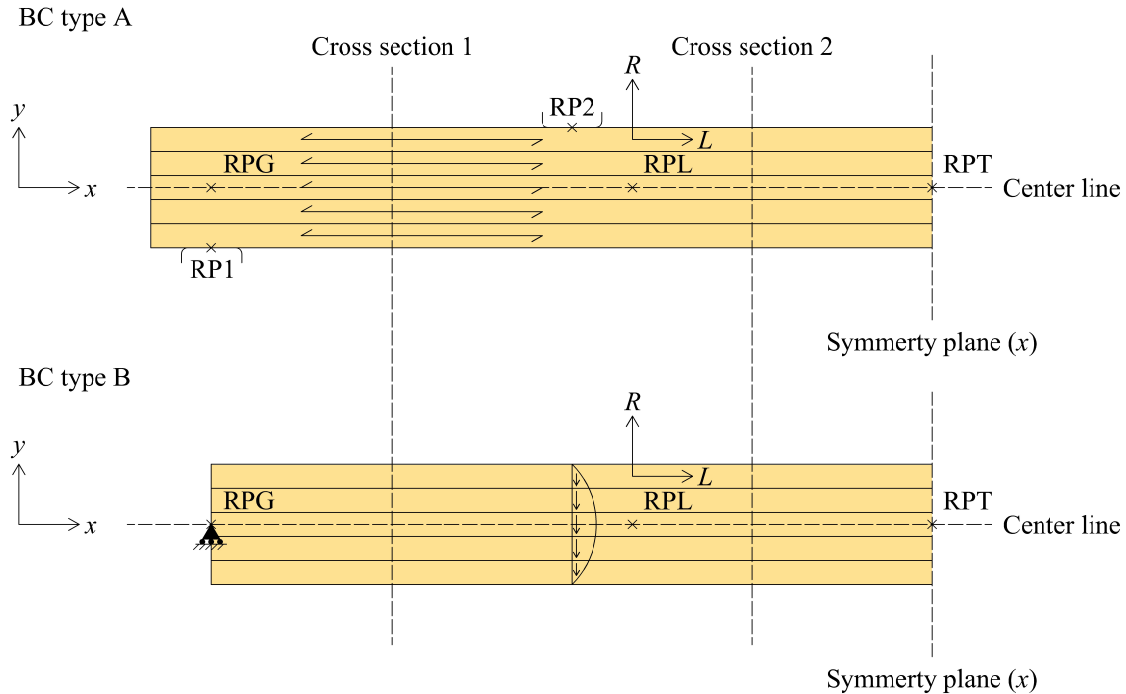


Figure 4.1: Sketch of homogeneous beams with laboratory and theoretical boundary conditions, BC type A and BC type B. Also showing the location of the cross sections 1 and 2.

Boundary conditions

When evaluating a homogeneous beam with varying longitudinal-tangential shear modulus, the results were analysed as the output/input-ratio in relation to the input longitudinal-tangential shear modulus. The results are displayed in Figure 4.2. As can be seen in the graph the output shear modulus is about 1.1 times larger than the shear modulus that was put into the models. This deviation was assumed to be the results of differences between the laboratory testing set-up compared to load case which the theory is based on. One major difference is the support and load application surface. To evaluate this the beam was modelled to resemble a Timoshenko beam, with theoretical boundary conditions. The difference in the output/input-ratio of the longitudinal-tangential shear modulus between the models that represent a laboratory test set-up and the models that represent Timoshenko beams is shown in Figure 4.2.

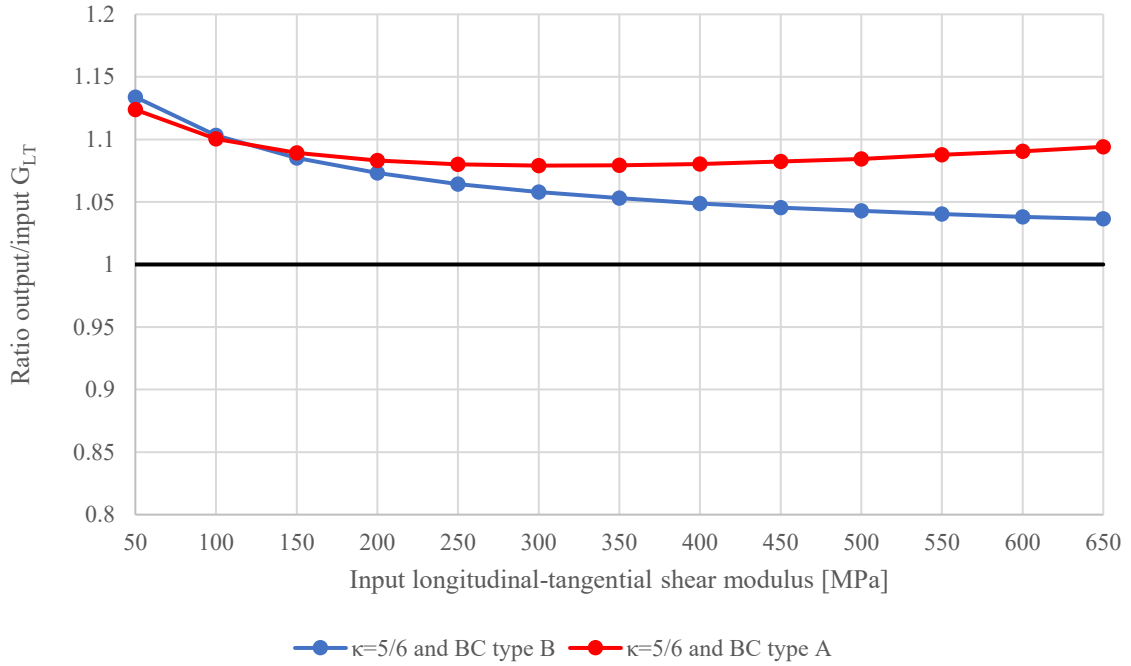


Figure 4.2: The difference of the output/input-ratio for beams with BC type A and BC type B in relation to the input. The beams were modelled as homogeneous with $\kappa=5/6$.

The results show that the effect of the difference between the boundary conditions is larger for beams with higher longitudinal-tangential shear modulus and then decrease as the shear modulus decrease. The results also show that the output is still not equal to the input, which indicates that there are other factors affecting the results. These other factors seem to affect the beam with lower shear modulus more than the beam with higher shear modulus, at least for BC type B.

Shear strain distributions

One of these factors was assumed to be the effect of shear strain distribution. To evaluate this the shear strain at the center line along the beams x -direction (see Figure 4.1) was extracted from the FE-models. This was done for both the model with boundary conditions representing the laboratory test set-up (BC type A) and the model with theoretical boundary conditions (BC type B). The extracted shear strains were then compared with the theoretical shear strains. The evaluation was done for the beams with the smallest and largest deviation between the output and the input, i.e. the beams with 650 MPa and 50 MPa as the input shear stiffness respectively. The results are showed in Figure 4.3 and 4.4.

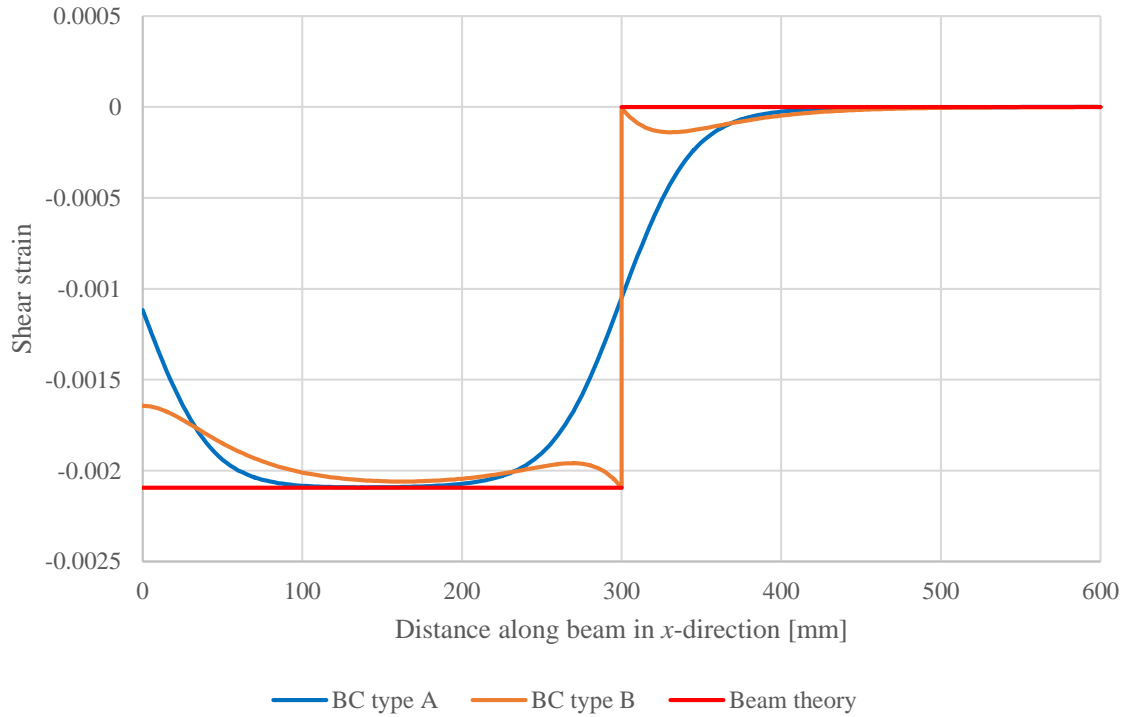


Figure 4.3: The difference between the shear strain along the center line of the beam according to theory and the FE-models with different boundary conditions. Results from beam with 650 MPa as the shear stiffness.

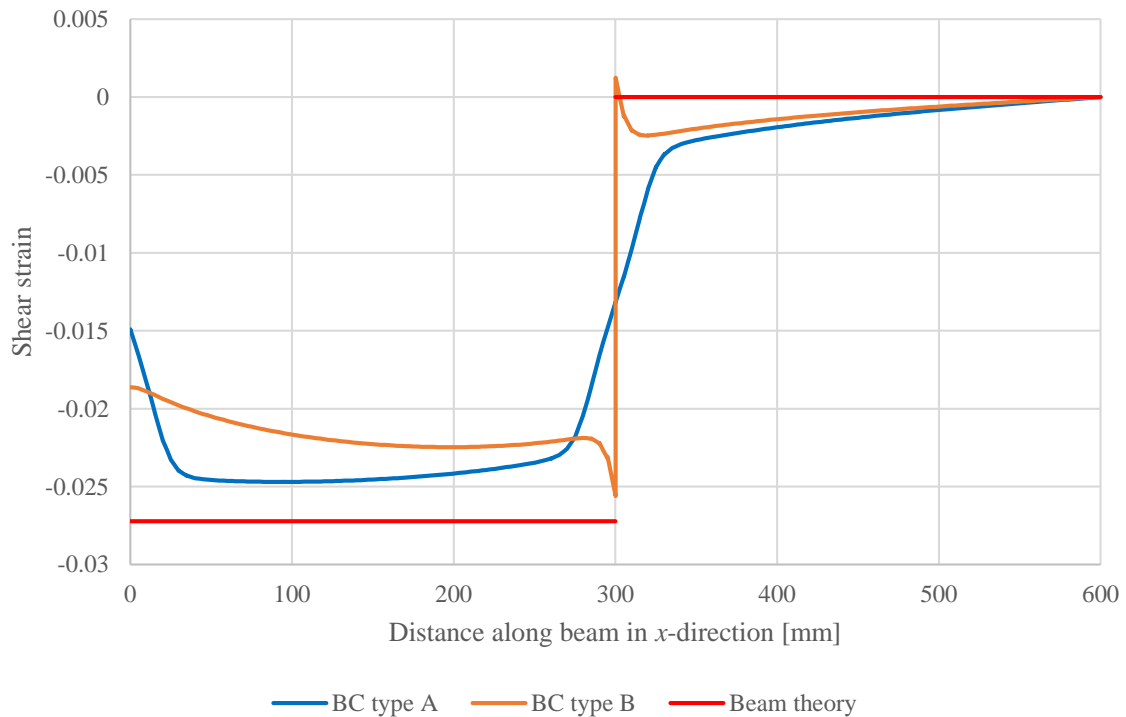


Figure 4.4: The difference between the shear strain along the center line of the beam according to theory and the FE-models with different boundary conditions. Results from beam with 50 MPa as the shear stiffness.

The shear strains from the FE-model in Figure 4.4 were obtained from the center line of the beam. To complete the understanding of the shear strain distribution over the height of the beam, the shear strains from two vertical cross sections were extracted from the FE-models. The first cross section is between the support and the load and the second one is between the load and the middle of the beam, see Figure 4.1. For the evaluated beams this represent $x=150$ mm and $x=450$ mm. The two cross sections are displayed in Figure 4.5 for a beam with 650 MPa as the input for the longitudinal-tangential shear modulus. The corresponding results for a beam with 50 MPa as the input for the longitudinal-tangential shear modulus are displayed in Figure 4.6.

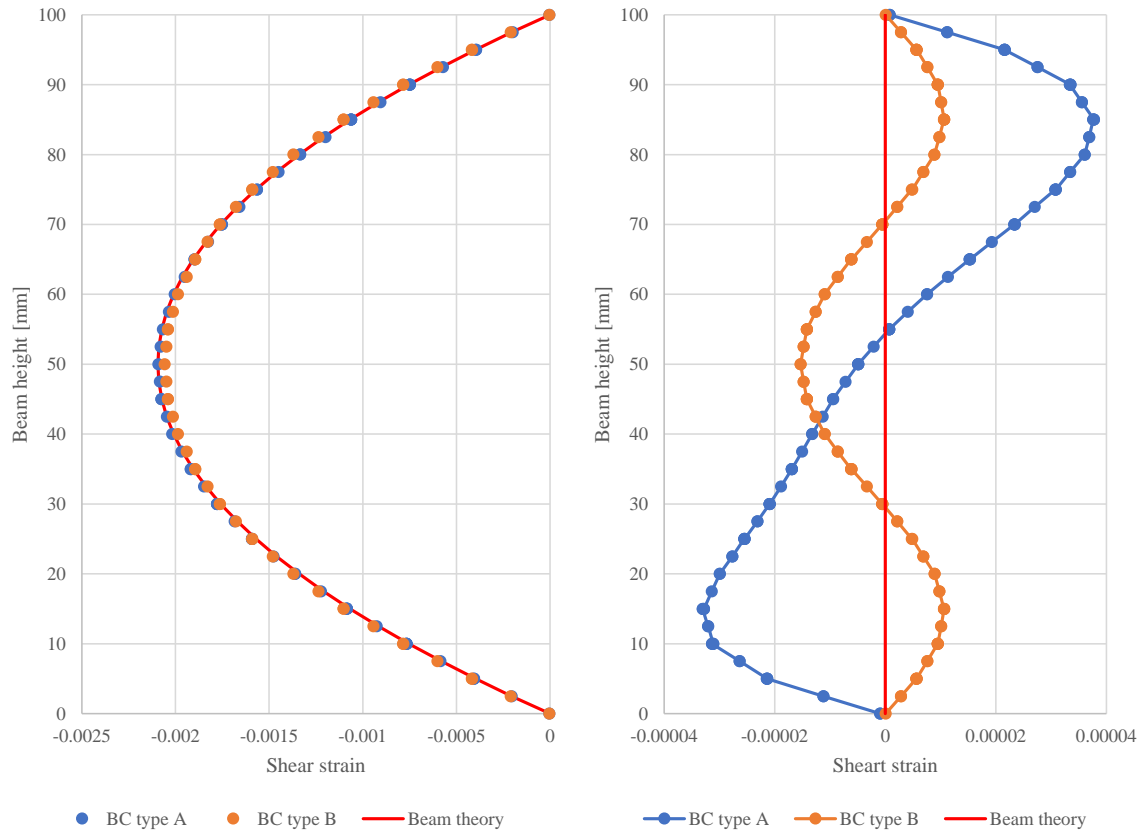


Figure 4.5: Shear strain distribution over the beam height at cross section 1 and 2 (see Figure 4.1). Beam with input longitudinal-tangential shear modulus $G_{LT} = 650$ MPa. Note the difference in scale between the two graphs.

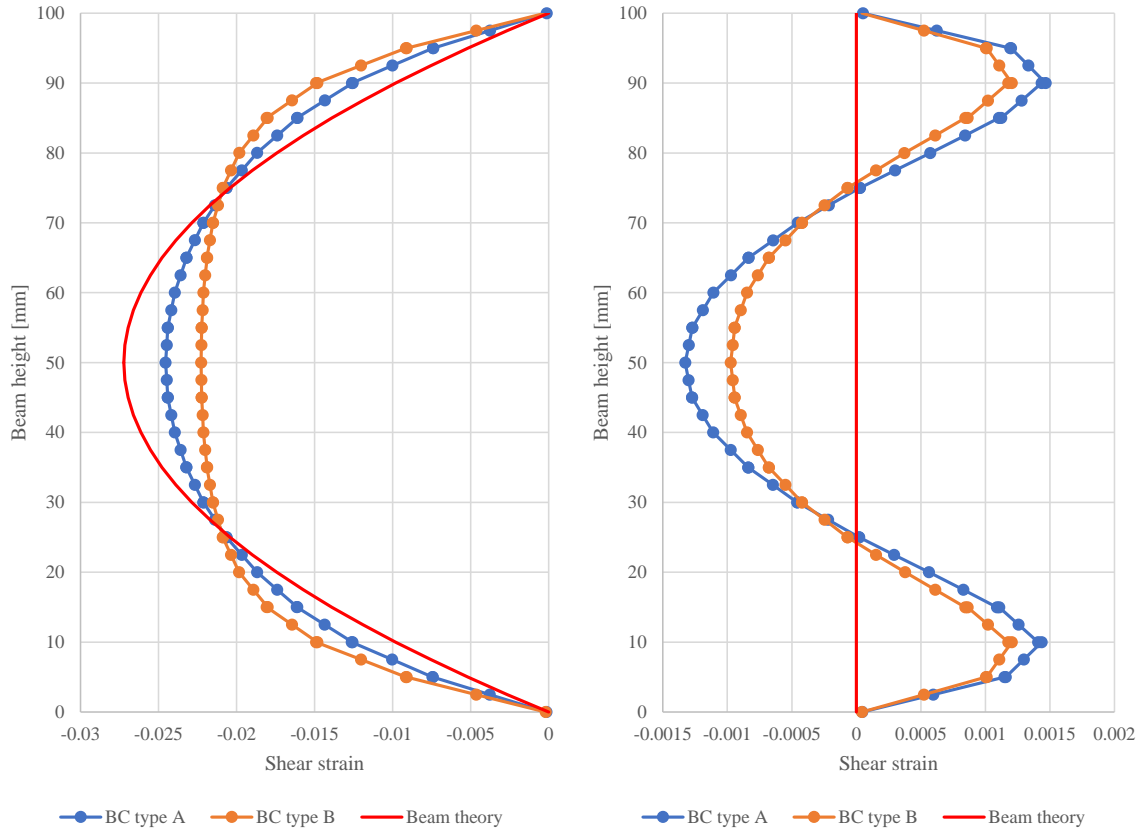


Figure 4.6: Shear strain distribution over the beam height at cross section 1 and 2 (see Figure 4.1). Beam with input longitudinal-tangential shear modulus $G_{LT} = 50$ MPa. Note the difference in scale between the two graphs.

The results from the analysis of the shear strains along the center line of the beams in Figure 4.3 and 4.4 indicate that the values from the FE-models vary compared to the shear strains according to Timoshenko beam theory. This was further proven by the analysis of the shear strain distributions over the height of the beams in Figure 4.5 and 4.6. Even though the results for the beam with the higher shear modulus ($G_{LT}=650$ MPa) correlate better with beam theory, both beams tend to deviate from theory between the load and the middle of the beam (between $x=300$ mm and $x=600$ mm in Figure 4.3 and 4.4).

This result was particularly interesting as the shear force between the two loads is zero. According to beam theory no shear force in turn leads to no shear stresses, no shear strains and no shear deflections. This was interesting to evaluate since the local deflections, which in turn are used to determine the local bending stiffness, are measured at this part of the beam at the reference point *RPG*. The equation used to determine the local bending stiffness is based on the assumption that the measured deflections only depend on bending deformations. As the results from the FE-models indicate that the local deflections are dependent on both bending and shear deformations, the measured local bending stiffness $(EI)_{local,net}$ deviates from the theoretical bending stiffness $E_L I_{net}$. This might be one of the reasons to the deviating results between the input and output of the shear modulus.

Improvement of testing method

These results lead to the investigation if the results would be improved if the reference length for the local bending stiffness l_1 was decreased to be less affected by shear strains and in turn shear deflections. As can be seen in Figure 4.3 and 4.4 the shear strains approaches the theoretical values closer to the middle of the beam. The influence of decreasing the length l_1 on the ratio of the measured and theoretical bending stiffness is displayed for a beam with 50 MPa and 650 MPa as the input shear modulus and BC type A in Figure 4.7.

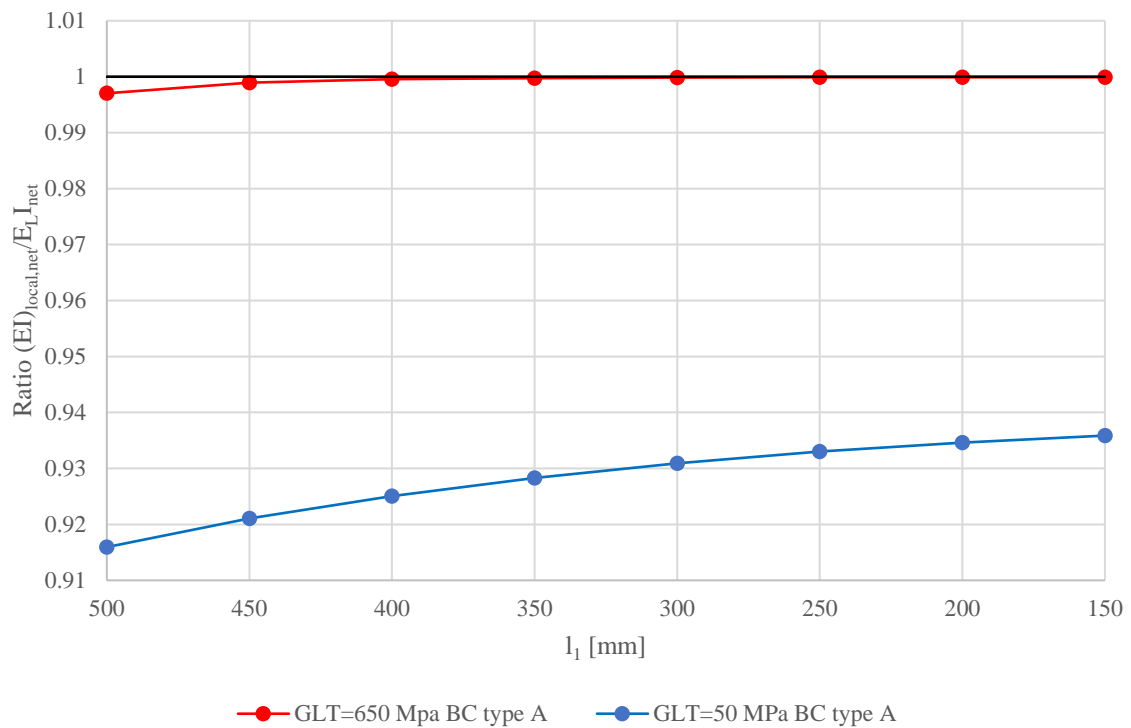


Figure 4.7: The ratio of the local bending stiffness determined with deflections from the FE-models (with BC type A) and the theoretical bending stiffness in relation to the reference length l_1 .

The results indicate that the measured local bending stiffness would be closer to the theoretical value if the length l_1 was decreased. For a beam with the longitudinal-tangential shear modulus of 650 MPa the results show that the local bending stiffness $(EI)_{local,net}$ converged towards the theoretical value when the length l_1 was decreased for a 1300 mm long beam. For beams with the same length but with lower longitudinal-tangential shear modulus (50 MPa), the determined local bending stiffness also came closer to the theoretical one as l_1 was decreased. The ratio between the two did however not converge towards one even if l_1 was decreased by 350 mm.

Before the alteration of l_1 the output/input-ratio of the longitudinal-tangential shear modulus was around 1.1 for the beam with 650 MPa as the input shear modulus. When decreasing l_1 to 300 mm the ratio of the output/input shear modulus decreased according to

$$\frac{G_{LT,output}}{G_{LT,input}} = \frac{690}{650} = 1.06 \quad (4.1)$$

4.1.2 CLT-beams

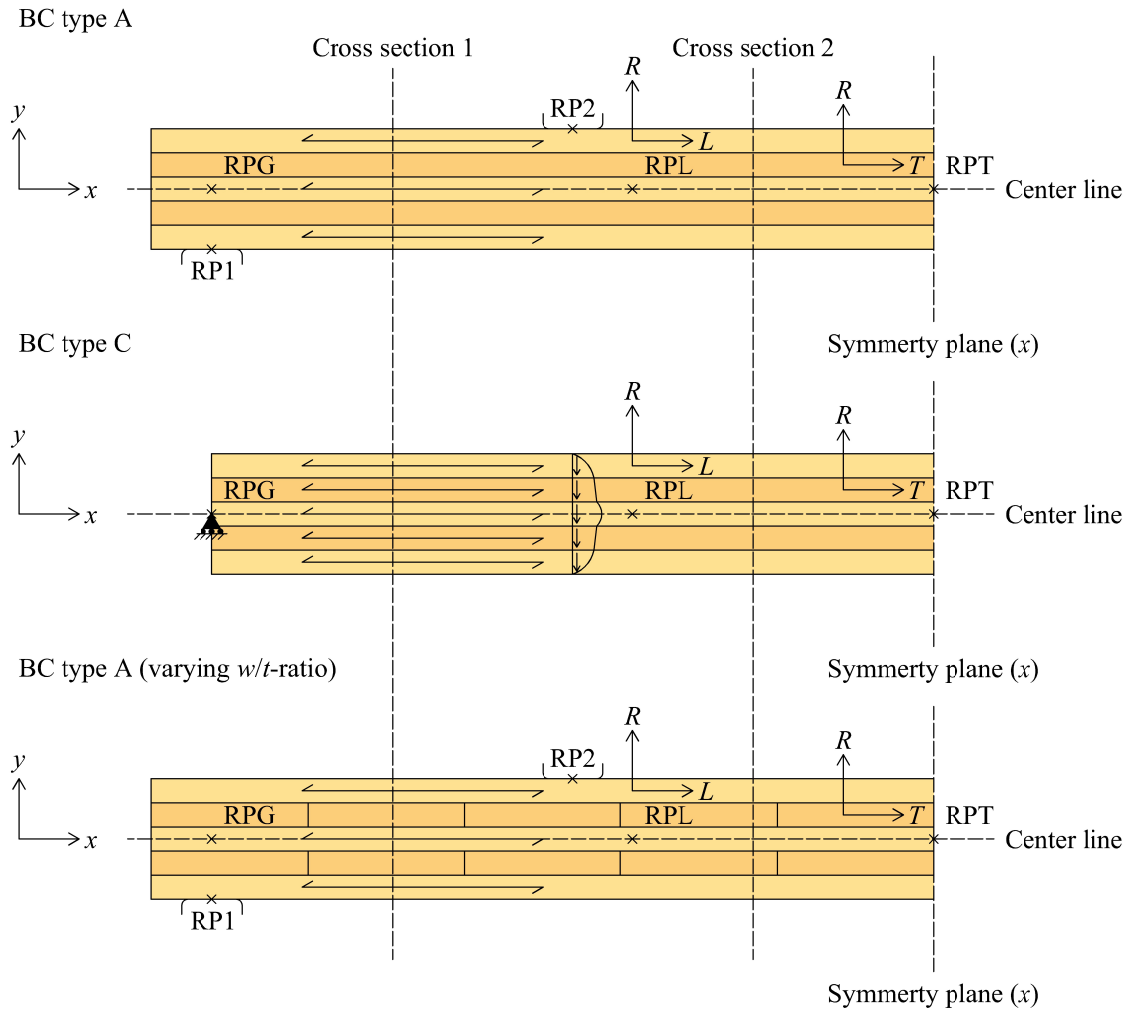


Figure 4.8: Sketch of CLT-beams with laboratory and theoretical boundary conditions, BC type A and BC type C. BC type A was evaluated with both homogeneous layers and with varying w/t -ratio. The sketch also shows the location of cross section 1 and 2.

Boundary conditions and shear correction factor

When the beam had been analysed as homogeneous, the transverse layers were implemented (see Figure 3.6). The results of the evaluation when comparing the output/input ratio of the rolling shear modulus in relation to the input for CLT-beams with homogeneous layers are displayed in Figure 4.9.

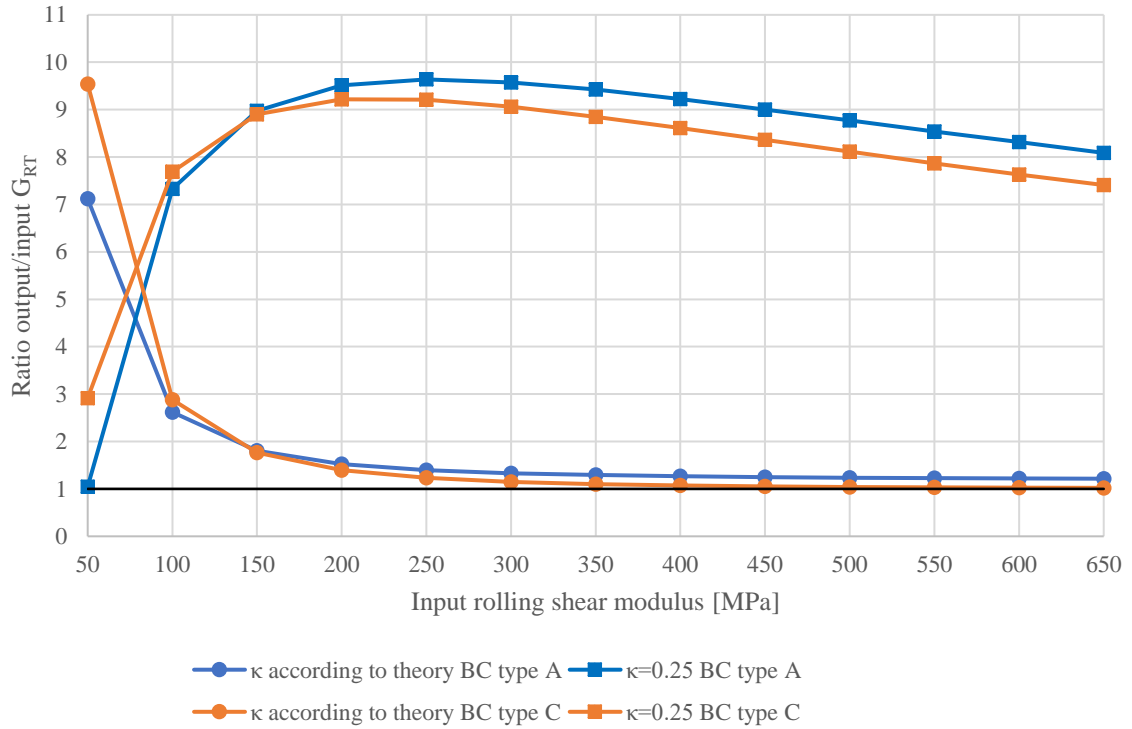


Figure 4.9: The output/input-ratio of the rolling shear modulus in relation to the input for beam with different shear correction factors and boundary conditions (BC type A and BC type C).

The blue lines in Figure 4.9 represent the output/input-ratio for the beams with boundary conditions representing a laboratory test set-up (BC type A), and the orange lines represent the beams analysed with theoretical boundary conditions (BC type C). The beams were first evaluated with the shear correction factor κ according to beam theory (see Equation 2.21). Both the blue and orange line (with dots) show large deviations for low rolling shear modulus G_{RT} , for an input value of 50 MPa the output value is around seven and nine times larger respectively for the two beam set-ups. These deviations were of significant interest as these are rolling shear properties often found in timber used for CLT. As the input was increased the output/input-ratio converged towards 1.2 for beams with BC type A and towards 1.0 for beams with BC type C. These results further prove the effect of the difference between the boundary conditions previously mentioned.

As mentioned in the preconditions, the shear correction factor could be set to 0.25, instead of the theoretical correction factor. This was tested and is represented by the blue and orange lines with squares in Figure 4.9. As can be seen in Figure 4.9 $\kappa = 0.25$ fits quite well for the beam with BC type A and the input rolling shear modulus of 50 MPa. If this isn't the case the accuracy of the outcome deviates beyond reasonable limits. This result indicates that if the rolling shear modulus is 50 MPa and the shear correction factor is set to 0.25 the testing method provides quite accurate results for this particular beam. The output/input-ratio was approximately 1.08 meaning that the result is 8 % larger than the actual rolling shear modulus, used as input in the FE-model.

Sensitivity of the testing method

The accuracy of the shear correction assumption was further evaluated for the model where the assumption seemed to fit best, i.e the model with BC type A and the input rolling shear modulus of 50 MPa. The accuracy and the sensitivity of the assumption was analysed by investigating the effect of a small deviation in the input rolling shear modulus. This was done by assuming that the rolling shear modulus of the test specimen was known to be 50 MPa with a deviation of 5 MPa. The shear correction factor was set to constantly 0.25. The results of a small deviation of the rolling shear modulus in relation to the output/input-ratio is shown in Figure 4.10.

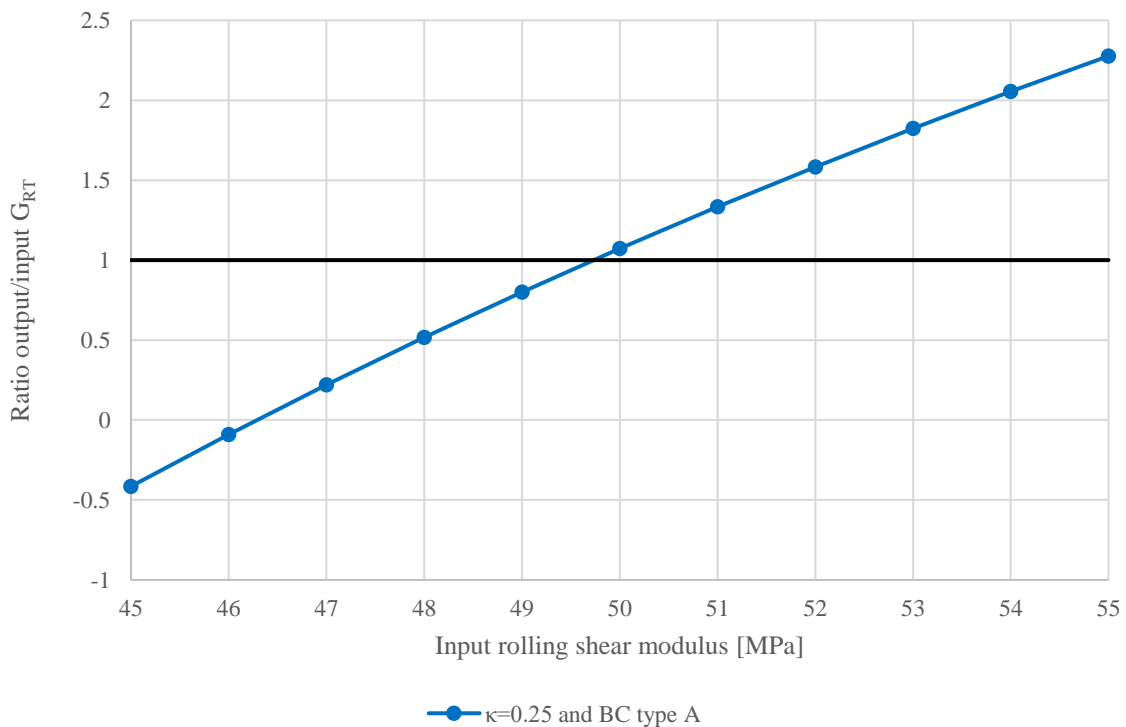


Figure 4.10: The output/input-ratio of the rolling shear modulus in relation to the input.

The results in Figure 4.10 show that if the input rolling shear modulus was set to 50 MPa the output would be approximately 54 MPa. This gives a output/input-ratio which is close to 1.0, meaning that the output is close to the input. If the input rolling shear modulus instead was set to 55 MPa the resulting output was ca 125 MPa. This result indicated that the testing method is very sensitive as an increase of the input by 8 % resulted in an increase of the output larger than 100 %. It also indicated that the accuracy of the assumption of the shear correction factor $\kappa = 0.25$ for beams with $G_{RT} = 50$ MPa might just be a coincidence.

Shear strain distributions

In addition to the evaluation of the factors affecting the equation used to determine the rolling shear modulus, the shear strains were also investigated for the CLT-beams. The evaluation was performed in a similar fashion as for the homogeneous beams, with the

corresponding cross sections and equal sets of boundary conditions. The shear strain distribution for CLT-beams with homogeneous layers with the input rolling shear modulus of 650 MPa and 50 MPa, at cross section 1 and 2 are displayed in Figure 4.11 and 4.12.

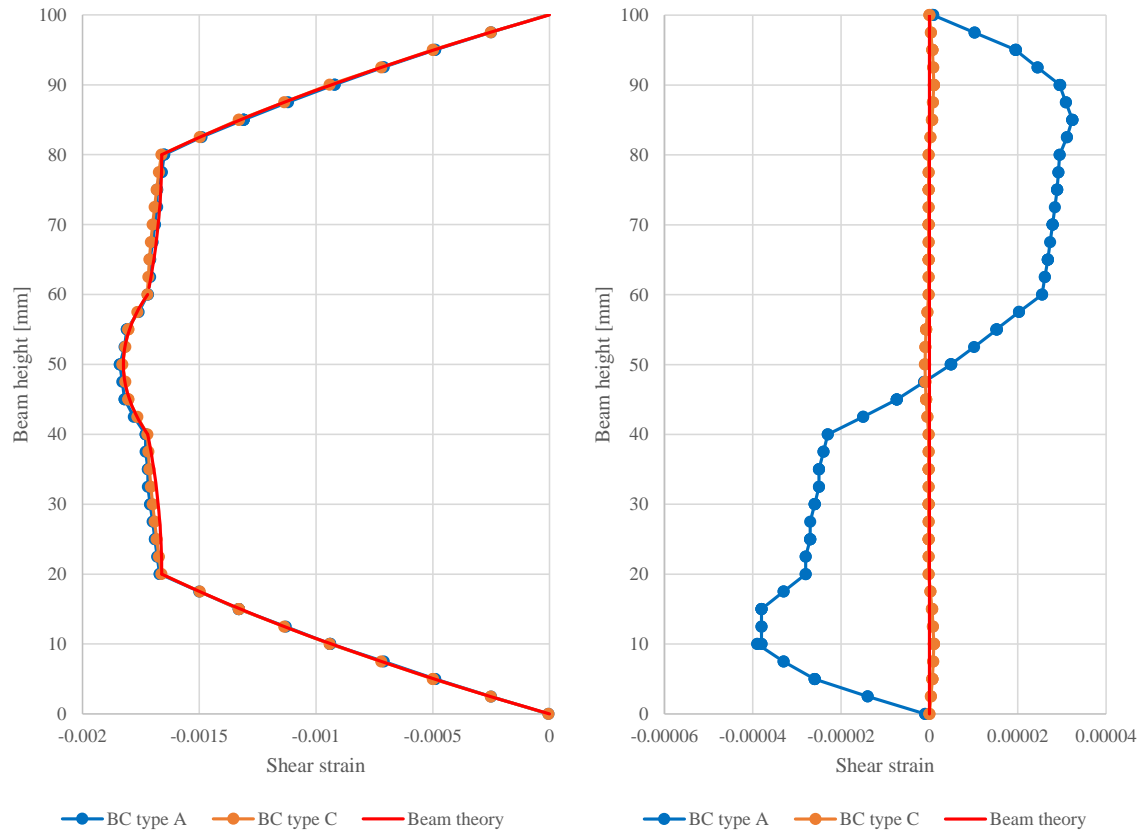


Figure 4.11: Shear strain distribution over the beam height at cross section 1 and 2 (see Figure 4.1). Beam with input rolling shear modulus $G_{RT} = 650$ MPa. Note the difference in scale between the two graphs.

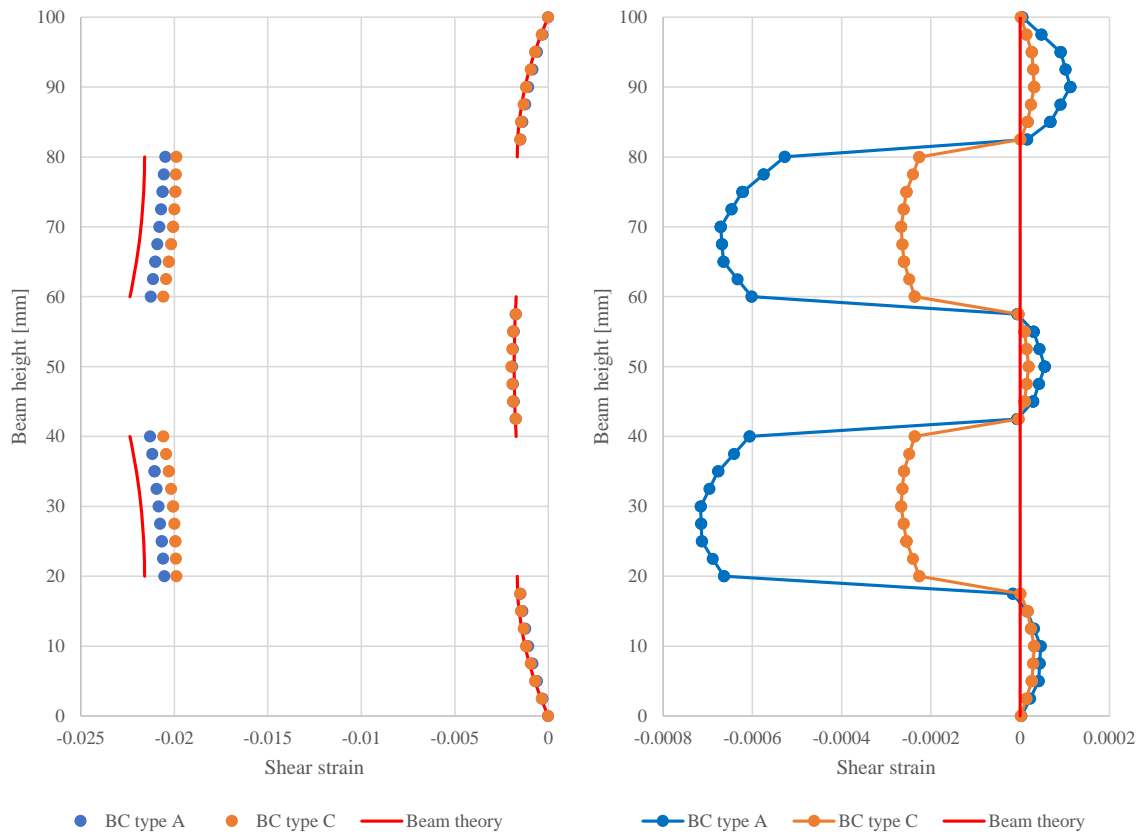


Figure 4.12: Shear strain distribution over the beam height at cross section 1 and 2 (see Figure 4.1). Beam with input rolling shear modulus $G_{RT} = 50$ MPa. Note the difference in scale between the two graphs.

The results show that just as for the homogeneous beam models, the shear strain distributions correlate better with Timoshenko beam theory at cross section 1 (between the support and load) compared to cross section 2 (between the load and the middle of the beam). The results also show that the shear strains for a beam with higher rolling shear modulus ($G_{RT} = 650$ MPa) correlate better with theory compared to a beam with lower rolling shear modulus ($G_{RT} = 50$ MPa). Especially interesting is the correlation at cross section 2, for the beam with higher rolling shear modulus and BC type C. The extracted shear strains from the FE-model were nearly zero over the beam height i.e. close to what Timoshenko theory assumes. This was not the case for any other beams analysed and explains why the output/input-ratio for this beam was closest to one (see Figure 4.9).

Annual growth ring pattern

The parametric study was finished with an evaluation of the effect of the annual growth ring pattern and the lamella width/thickness-ratio. Even though the results of the test method is largely influenced by beam theory assumption, these parameters are of interest as they affect the bending of beam. Previous research suggests that the output rolling shear modulus from a similar FE-model can be 1.4 to 2.8 times higher than the input for various annual ring configurations [16].

The effect of the annual growth ring pattern was analysed by altering the curvature of the rings. The curvature is dependent on where the lamella is sawn on a tree log. The further away from the pith, the flatter the curvature of the annual growth rings are (see Figure 3.7). The effect of how the distance to the pith c affected the output/input-ratio is shown in Figure 4.13. The models tested had an input rolling shear modulus of 50 MPa, BC type A and a lamella width/thickness ratio of 6.5 with glued edges (see bottom sketch in Figure 4.8).

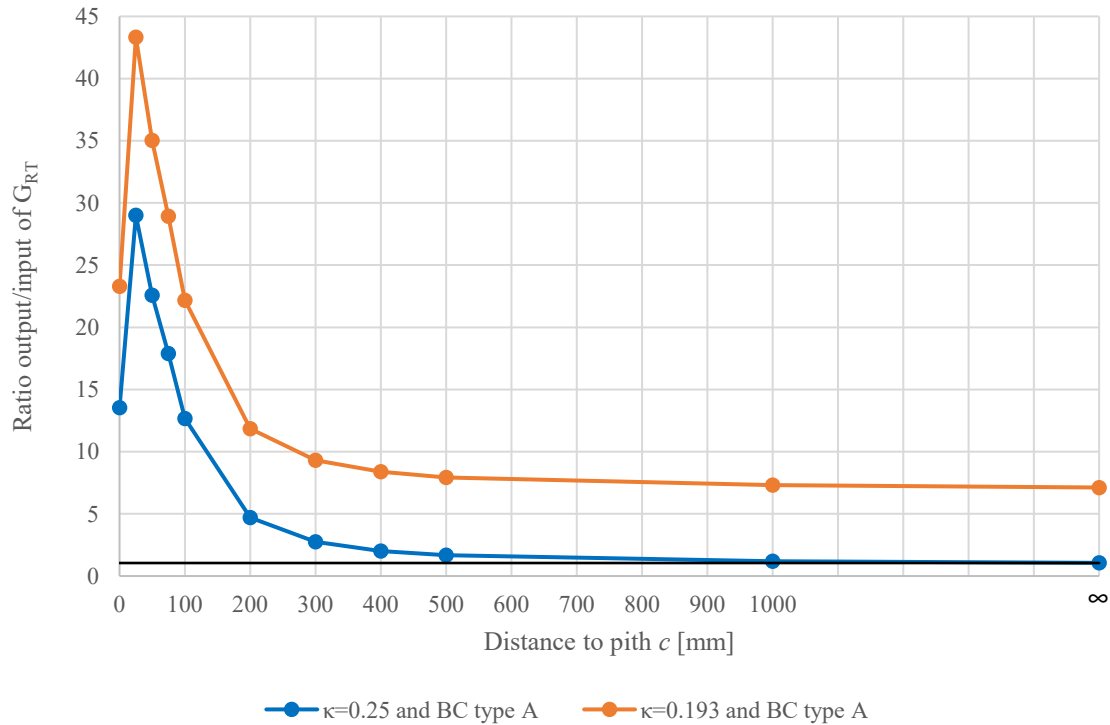


Figure 4.13: The output/input-ratio of the rolling shear modulus in relation to the distance to the pith c . BC type A and w/t -ratio=6.5.

As can be seen in Figure 4.13, the annual growth ring pattern has a large influence on the output/input-ratio of the rolling shear modulus. The results show that when the distance to the pith c is shortened the output rolling shear modulus is significantly higher than the input. The increased curvature of the annual growth rings was beforehand expected to increase the shear stiffness of CLT, just as the results show. The magnitude of the effect is thought greater than expected. As the accuracy of the output/input-ratio tends to deviate even when the annual growth rings were not implemented, it might be difficult to draw any conclusion from these results.

When the distance from the pith then increases, meaning less curved annual growth rings, the output/input-ratio converges towards one for analysis with the alternative shear correction factor ($\kappa = 0.25$) and around seven for analysis with the shear correction factor according to theory ($\kappa = 0.193$). These results correlate with the results shown in Figure 4.9 (see the blue line with squares ($\kappa = 0.25$) and the blue line with dots ($\kappa=0.193$) at input value $G_{RT} = 50$ MPa).

Lamella width/thickness ratio

Finally the effect of the relation between the width and thickness of the transverse lamellas on the output/input-ratio of the rolling shear modulus was evaluated. The evaluated models had an input rolling shear modulus of 50 MPa, BC type A and non glued edges (see bottom sketch in Figure 4.8). As mentioned previously the actual magnitude of this effect might be difficult to determine as the testing method tends to be largely affected by other factors concerning beam theory assumptions. The results shown in Figure 4.14, indicate that the width/thickness-ratio affects the rolling shear modulus as expected. The larger the width of the transverse lamellas the higher the rolling shear modulus.

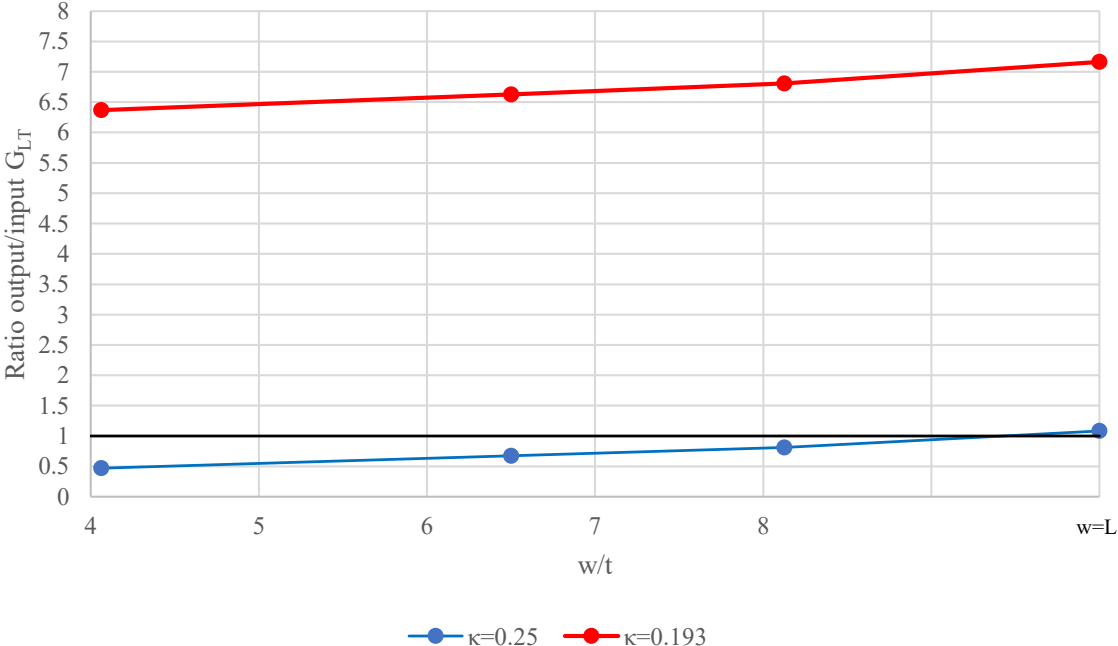


Figure 4.14: The output/input-ratio of the rolling shear modulus in relation to the lamella width/thickness-ratio. BC type A.

5 Discussion and Conclusions

5.1 Concluding remarks

The aim and objective of this dissertation was to thoroughly evaluate the four-point bending test which is described in the Europe Standard EN 16351. The aim was also to do a parametric study where parameters such as lamella thickness/width-ratio and annual growth ring orientation would be evaluated. As the project proceeded, new factors and parameters that affected the results significantly were discovered. These new factors concerned the differences between laboratory tests (represented by FE-models) and beam theory assumptions and had to be evaluated before specific parameters concerning CLT could be evaluated.

The FE-model was first modelled to resemble a laboratory test set-up as much as possible and was modelled as a CLT-beam (see Figure 3.6). When determining the output rolling shear stiffness based on measurements from this model, the output deviated significantly from the input. This led to a step-wise simplification of the model to eventually represent a theoretical Timoshenko beam. The first step was to remove the transverse layers and evaluate a homogeneous beam with all layers in the longitudinal direction (see Figure 3.5). The purpose of this was to reduce the theoretical assumptions affecting the equation for the output shear modulus. In particular the shear correction factor which is constant for homogeneous rectangular beams. The results between the input and output from this evaluation still deviated, which led to the conclusion that further factors affected the results.

Remarks on boundary conditions

A part of the simplification was to remove the modelled support and load application surface and replace them with theoretical boundary conditions. The purpose of this was to evaluate the effect of the difference between the theoretical and laboratory boundary conditions. The results for the homogeneous beams (see Figure 4.2) showed that the difference between the output- and input shear stiffness was reduced a bit for the beams evaluated with higher input longitudinal-tangential shear modulus. The beams with low shear stiffness were less affected by the boundary conditions. This led to the conclusion that the boundary conditions do affect the results, but the beams with low shear stiffness are predominantly affected by other factors. The same results were obtained for the CLT-beams (see Figure 4.9).

When executing this test in a laboratory the beam will likely be placed on two supports with a certain width and the two loads will be applied by some sort of steel beam which also has a certain width. These widths might lead to different boundary conditions than what theory assumes. The loads may act as distributed over the widths of the

steel beams rather than point loads. This is not accounted for in beam theory. In theory the support is placed at the mid height of the beam in a single point and the load is applied in a single point also at the center line of the beam. These differences might explain the deviating results between beam theory and the FE-models.

Remarks on shear strain distributions

Even when the boundary conditions for the FE-models were altered to resemble Timoshenko beam theory, the output- and input shear modulus deviated (see Figure 4.2 and 4.9). To evaluate this deviation further the shear strain distributions of the beams with the highest and lowest shear stiffness were evaluated. The measured shear strains turned out to deviate from the theoretical ones. This was also the case between the load and the middle of the beam where the shear strains according to beam theory are zero. As the shear strains at this part of the beam deviated from zero, it affected the measurement of the local deflections. The local deflections, used to determine the local bending stiffness, was therefore not only dependent on bending deformations as the method assumes (see Section 2.4.1). The inaccuracy of the local bending stiffness in turn lead to inaccurate output of the shear modulus.

Remarks on shear correction factor

When evaluating the FE-models representing CLT-beams the output rolling shear modulus deviated significant from the input values (see Figure 4.9). The deviation for the input value of 50 MPa, which is the typical rolling shear modulus for C24, turned out to deviate the most. The output was around seven times larger than the input with BC type A. This result was obtained with the shear correction factor according to beam theory. The preconditions according to EN 16351 though state that the correction factor may be set to $\kappa = 0.25$. With this alteration the output/input-ratio of the rolling shear modulus was improved significantly for this beam.

The improvement was however only detected for the case when the input was 50 MPa. A small deviation from 50 MPa showed a large deviation of the output. The conclusions drawn from this is that the choice of the shear correction factor affects the results significantly and in order to do a suitable choice the input rolling shear modulus must be known beforehand.

The results also showed how a small change of the input results in a relatively large change of the output (see Figure 4.10). Consider the test to be executed in a laboratory with a real CLT-beam and the rolling shear modulus is assumed to be 50 MPa. The shear correction factor is then set to 0.25 as described in the preconditions according to EN 16351. If the actual value of the rolling shear modulus is 55 MPa, which is a reasonable deviation, the outcome of the test would be more than twice as large deviation then what can be expected. This indicates that the testing method is sensitive to small deviations which would be hard to avoid in practice.

Remarks on the sensitivity of the testing method

One of the reasons why the testing method is sensitive to small errors is to be found in the equation used to determine the shear modulus of the entire cross section (see Equation 2.37). In the denominator of that equation the difference between the local and the apparent bending stiffness is used as a factor. A local bending stiffness deviating just one percent results in a far greater deviation of the shear stiffness and, in turn, results in an inaccurate value of the rolling shear modulus.

Remarks on annual growth ring orientation

The evaluation of the annual growth ring orientation was performed on beams with the input rolling shear modulus of 50 MPa with both the theoretical and altered shear correction factor. The results showed that the annual growth ring pattern had a large impact of the output/input-ratio of the rolling shear modulus. The more curvature the annual rings had the more the ratio was affected. This outcome was also expected based on previous research. Conclusions can be drawn that the annual ring pattern affects the shear stiffness of CLT, the magnitude of that effect is ,however, difficult to determine due to the uncertain accuracy of the testing method.

Remarks on lamella width/thickness-ratio

The evaluation of the width/thickness-ratio of the transverse lamellas was performed on beams with the input rolling shear modulus of 50 MPa with both the theoretical and altered shear correction factor. The same conclusions as for the evaluation of the annual growth ring pattern was drawn from this evaluation. The lamella width/thickness-ratio ultimately affects the bending of the beam and in turn affects the measurements, but no conclusion of the magnitude of this effect can be drawn.

Final remarks

A source of error in this project might be the fact that the testing method was evaluated with FE-models and not real CLT-beams as the preconditions stated. The FE-models were modelled to resemble real life beam as much as possible, but will of course deviate from reality. In this project this was although rather an advantage than a disadvantage. For instance a real CLT-beam will have far more initial deformations, irregularities and other unexpected factors that influence the results. And consider the fact that the testing method is rather sensitive, achieving accurate results with a real beam would be even harder than for a FE-model. An other advantage with the modeling is that the actual rolling shear modulus is known beforehand since it is used as an input parameter. For a real beam this wouldn't be the case which for example complicates the choice of the previously mentioned shear correction factor.

To summarize, the results of this project indicate that the testing method needs to be

further evaluated to be a reliable source to determine the rolling shear modulus of CLT. The method will be difficult to use in practice since it requires such precise measuring due the sensibility. And even if the measuring is done correctly the outcome might not be the expected one. The outcome is heavily influenced by both beam theory assumptions and outer assumptions like the input rolling- and longitudinal-tangential shear modulus. Some of the assumptions made require a valid guess of what the outcome will be. If the wrong assumptions are made the outcome will be more or less irrelevant to use since it deviates far from the real outcome.

5.2 Further analysis

When evaluating the testing method in this project the outcome deviated far from what was expected beforehand. The results indicate that this was due to the differences between assumption within Timoshenko beam theory and the deformation patterns found from the FE-models. A further analysis of the testing method could be to investigate potential improvements of the method.

When evaluating the shear strains along the length of the beams (see Figure 4.3 and 4.4), the results showed that the shear strains deviated more close to the load compared to the middle of the beam. The effect of moving the reference point for the local deflections RPL closer to the middle was therefore evaluated. The results showed that the measured local bending stiffness came closer to the theoretical bending stiffness as RPL was moved closer to the middle. This suggests that the testing method might be improved by reducing the reference length for the local deflection l_1 . Further changes of this type can be evaluated. For instance how the test set-up should look like and where the deflections should be measured to decrease the influence of theoretical and practical differences even more.

The assumptions within the beam theories considered in this work could also be further evaluated. A thorough evaluation of the shear correction factor κ would be interesting. Both a more detailed evaluation of how the factor is determined and how this could be used to better understand and improve the testing method. Based on the results from this project, such an evaluation would be essential to validate this test method as reliable.

Further analysis could also be to evaluate the testing method with real CLT beams. This is essentially what the testing method is developed for. This project was based on FE-models that gives approximate solutions which might deviate from reality. These possible deviations between real CLT-beams and FE-models can be further evaluated, both to improve the FE-models and to gain further understanding of the testing method. The effect of other parameters such as imperfection could also be evaluated for real beams.

Bibliography

- [1] Swedish Wood. *The CLT Handbook*. Skogsindustrierna Svenskt Trä, 2019. ISBN: 978-91-983214-4-3.
- [2] R Brandner, G Flatscher, A Ringhofer, G Schickhofer and A Thiel. “Cross laminated timber: overview and development”. In: *European Journal of Wood and Wood Products* 74.3 (2016). DOI: 10.1007/s00107-015-0999-5.
- [3] *CE-märkning*. Accessed: 2022-03-30. URL: `\url{https://www.sis.se/standarder/ce-markning/}`.
- [4] *EAD-130005-00-0304 – Solid wood slab element to be used as a structural element in buildings*. 2015. URL: https://www.eota.eu/download?file=/2013/13-13-0005/ead%20for%20jeu/ead-130005-00-0304-solid-wood-slab-element-structural-element-in-buildings_jeu.pdf.
- [5] *EN 16351 – Timber structures – Cross laminated timber – Requirements*. 2021. URL: <https://www.sis.se/produkter/trateknik-15e6ae2b/trabaserade-skivor/plywood/ss-en-163512021/>.
- [6] Swedish Wood. *Design of timber structures*. Swedish Forest Industries Federation, 2016. ISBN: 978-91-980304-8-8.
- [7] Ingela Bjurhager. *Effects of Cell Wall Structure on Tensile Properties of Hardwood*. KTH Royal Institute of Technology, 2011. ISBN: 9789174159141.
- [8] F Nilsson, C Roberge and J Fridman. *Forest statistics 2021*. Brochure. 2021. URL: https://www.slu.se/globalassets/ew/org/centrb/rt/dokument/skogsdata/skogsdata_2021_webb.pdf.
- [9] Peter A. Classie. *Civil Engineering Materials*. Wings Books New York, 2016. ISBN: 9780128027516.
- [10] T Ehrhart and R Brandner. “Rolling shear: Test configurations and properties of some European soft/and hardwood species”. In: *Engineering structures* (2018). DOI: 10.1016/j.engstruct.2018.05.118.
- [11] Kent Persson. *Micromechanical Modelling of Wood and Fibre Properties*. PhD. Thesis. 2000. DOI: 10.13140/RG.2.1.1389.7685.
- [12] Hasslacher Norica Timber. *Cross Laminated Timber Birch*. Brochure. 2021. URL: https://www.hasslacher.com/data/_dateimanager/broschuere/HNT_News_Birke_BSP_EN_Web.pdf.
- [13] Franke Steffen. “Mechanical properties of beech CLT”. In: *WCTE 2016 – World Conference on Timber Engineering*. 2016. URL: https://www.researchgate.net/publication/312198447_MECHANICAL_PROPERTIES_OF_BEECH_CLT.
- [14] Simon Aicher, Zachary Christin and Maren Hirsh. “Rolling shear modulus and strength of beech wood laminations”. In: *Holzforschung* 70.8 (2016), pp. 773–781. DOI: 10.1515/hf-2015-0229.

- [15] P Fellmoser and H J Blas. *Influence of rolling shear modulus on strength and stiffness of structural bonded timber elements*. Paper. 2004. URL: <https://holz.vaka.kit.edu/public/40.pdf>.
- [16] Emil Nilsson. *Characterisation of Cross laminated Timber properties*. Master Dissertation. 2021. URL: <https://www.byggmek.lth.se/fileadmin/byggnadsmekanik/publications/tvsm5000/web5250.pdf>.
- [17] G Fink, J Kohler and R Brandner. “Application of European design principles to cross laminated timber”. In: *Engineering structures* 171 (2018), pp. 934–943. DOI: 10.1016/j.engstruct.2018.02.081.
- [18] Dietrich Buck. *Mechanics of Cross-Laminated Timber*. Luleå University of Technology, 2018. ISBN: 978-91-7790-151-8.
- [19] Unknown. *Balkteori*. KFS AB, 2020.
- [20] C Ha-Minh, Dong Van Dao, F Benboudjema, S. Derrible, Dat Vu Khoa Huyn and Anh Minh Tang. “A Current-State-of-the-Art on Design Rules Vs Test Resistance of Cross Laminated Timber Members Subjected to Transverse Loading”. In: *CIGOS 2019, Innovation for Sustainable Infrastructure*. 2019. URL: <https://rdcu.be/cN7Ey>.
- [21] *SS-EN 408:210+A1:2012*. 2012. URL: <https://www.sis.se/produkter/byggnadsmaterial-och-byggnader/byggnadsstommar/trakonstruktioner/ssen408/>.
- [22] P-E Austrell, O Dahlblom, J Lindemann, A Olsson, K-G Olsson, K Persson, H Petersson, M Ristinmaa, G Sandberg and P-A Wernberg. *CALFEM - A finite element toolbox*. Structural Mechanics, LTH, Sweden, 2004.
- [23] *Mesh Convergence*. Accessed: 2022-04-12. URL: <https://abaqus-docs.mit.edu/2017/English/SIMACAEFSARefMap/simagsa-c-ctmmeshconverg.htm>.